Intertidal Regions Regulate Seasonal Coastal Carbonate System Dynamics in the East Frisian Wadden Sea

Julia Meyer^{1, 3}, Yoana G. Voynova¹, Bryce Van Dam¹, Lara Luitjens², Dagmar Daehne², Helmuth Thomas^{1, 3}

- ¹ Institute of Carbon Cycles, Helmholtz-Zentrum Hereon, Geesthacht, 21502, Germany-5
 - ² Lower Saxony department of water management, coastal protection and nature protection (NLWKN), Norden, 26506, Germany
 - ³ Institute for Chemistry and Biology of the Marine Environment (ICBM), Carl von Ossietzky Universität Oldenburg, 26111 Oldenburg, Germany
- 10 Correspondence to: Julia Meyer (julia.meyer@hereon.de)

Abstract. Seasonal and regional changes in carbon dynamics in the Wadden Sea, the world's largest intertidal sand and mud flats system, were analyzedanalysed to quantify the influence of biogeochemical processes (CaCO₃ dissolution and formation, photosynthesis, respiration) on the carbonate system at the land-sea interface. With a focus on the East Frisian Wadden Sea and the highly turbid Ems River estuary, (EFWS), we successfully implemented the proxy of used the difference between total alkalinity (TA) and dissolved inorganic carbon (DIC) ([TA-DIC]), as well as the calculated parameters ΔTA_{excess}, ΔDIC_{excess} and ΔTA_P to identify how ongoing biogeochemical processes regulate the carbonate system dynamics—and the land-sea interface.

In spring, a phytoplankton bloom with high biological activity—was, indicated by (a) supersaturated oxygen (up to 180 in % saturation), (b) elevated chlorophyll *a* (up to 151.7-μg- μg L⁻¹) and (c) low *p*CO₂ (as low as 141.3-μatm). As a result, μatm), resulted in decrease in nitrate (NO₃-,NO₃-, 19.29 ± 18.11 μmolμmol kg⁻¹)-1 and DIC (159.4 ± 125.4 μmolμmol kg⁻¹) decreased, whereas—1), and a slight increase in TA slightly increased (9.1 ± 29.2 μmolμmol kg⁻¹) in the intertidal regions from March 2022 to May, most likely through nitrate assimilation.—1). The regression analysis of the 20-differences between March and May 2022 in NO₃- concentrations (ΔNO₃-) against the differences in DIC (ΔDIC) between March and May 2022 yielded a slope of 6.90 which is close to matching the Redfield ratio of 6.625 for the C:N ratio of freshly produced phytoplankton biomass, and suggesting that uptake of nitrate by primary producers increased total alkalinity during the spring bloom.

In summer, high seasonal TA values (up to 2400 μmol kg⁻¹) in the Western part of the East Frisian Wadden Sea, along with positive ΔTA_{excess} at 73.3 % of all stations, indicated production of TA during this season in the intertidal regions, complemented the DIC dynamics. In summer, we assume that organic matter remineralization, along with CaCO₃ dissolution in sediments, enhances TA production in the coastal and nearshore regions of the Western EFWS (up to 2400 μmol kg⁻¹). In the Eastern EFWS, enhanced CaCO₃ formation may consume TA ([TA-DIC] < 200 μmol kg⁻¹), but the region still acts as a net source of TA, likely due to sedimentary processes such as organic matter decomposition, which follow the time of increased biological activity during the spring bloom. The increase of TA enhances the coastal ocean's ability to absorb and store CO₂

through buffering, chemical equilibrium, biological calcification and the carbonate pump, and suggests that the intertidal regions EFWS can be a source of total alkalinity TA to the coastal regions during the warm productive seasons. The This study highlights the complex relationships of these factors, emphasizing the need for a comprehensive understanding of regional and seasonal variations to better assess the role of coastal systems in carbon cycling, storage and climate regulation.

1 Introduction

35

40

50

Coastal oceans are biogeochemically active regions, which play a significant role in biogeochemical cycles, despite covering less than 10 % of the oceanic realm (Gattuso et al., 1998). Coastal regions are directly affected by input of terrestrial organic matter and nutrients through river run-off and, groundwater discharge and, atmospheric deposition, withand exchange of large amounts of matter and energy with the open ocean (Borges et al., 2006; Gattuso et al., 1998). Overall, coastal oceans also support approximately 14—23 % of the ocean carbon dioxide uptake, 10—30 % of the primary production, 80 % of organic matter burial, 90 % of sedimentary mineralization and 75—90 % of the oceanic sink of suspended river loads (Bauer et al., 2013; Gattuso et al., 1998).

For yearsSince the start of the industrial era, the levels of CO₂ in the atmosphere have been increasing increased from ~280 ppm in the preindustrial period to over ~419 ppm due to human activities (Friedlingstein et al., 2023). About). The uptake of atmospheric CO₂ by the ocean, estimated to about 30 % of the anthropogenic CO₂ emissions since the industrial period have been absorbed by the ocean (Friedlingstein et al., 2023). The uptake increases the concentration of), causes an increase in protons [H⁺]⁺] and a decrease of decreases the carbonate ion concentration [CO₃²], which CO₃²], leading to lower the pH and a reduced saturation state of calcium carbonate, a process known as ocean acidification (Orr et al., 2005). Depending on the different model scenarios, it is predicted that surface pH in the ocean might decline by about 0.3—__0.4 pH units by 2100, corresponding to a decrease of about 40—__50 % of carbonate ions in the seawater (Feely et al., 2009; Orr et al., 2005). The future capacity of the ocean to take up CO₂, can affect the precipitation and dissolution of the carbonate minerals, as well as the survival of marine organisms ((Duan et al., 2023; Kroeker et al., 2013; Liang et al., 2023; Ricour et al., 2023). Whereas oceans are a significant sink for anthropogenic CO₂; it is not well known how this uptake will further change under the continual increase of anthropogenic CO₂ in the atmosphere ((Lorkowski et al., 2012; Sabine et al., 2004; Thomas et al., 2007).) However, rising atmospheric CO₂ will influence carbon stocks and fluxes in the pelagic, benthosbenthic and coastal zone, particularly in shelf seas, which are annually mixed and ventilated (Legge et al., 2020).)

Total alkalinity (TA) represents the buffering capacity of the ocean and is controlled by many factors including erosion/weathering processespathways on land (Lehmann et al., 2023) and respiration of organic matter (OM) along anaerobic metabolic processespathways, mostly generated in shallow marine and shelf sediments (Dickson, 1981)...). These processes are directly influenced by terrestrial and anthropogenic nutrient inputs (Van Beusekom and De Jonge, 2002; Burt et al., 2016; Thomas et al., 2009), as well as and by increased sedimentation of reactive organic matter (OM) (Al-Raei et al., 2009; Böttcher et al., 1998)...). Coastal seas and shelf seas, like the North Sea often have relatively high rates of primary production in spring,

leading to drawdown in DIC, *p*CO₂ and a consequent pH increase (Macovei et al., 2021; Thomas et al., 2005), 2005a). In addition, nutrient loads from land ean-contribute to enhanced primary production, and increased carbon remineralization (Thomas(Prowe et al., 2009; Thomas et al., 2009), and subsequent changes in the carbonate system. In addition, there have beenPrevious studies (Thomas et al., 2009; Voynova et al., 2019), which suggestsuggested that intertidal regions like-the Wadden Sea-can play, a large network of intertidal sand and mudflats bordering the North Sea along the Dutch, German and Danish coasts (Staneva et al., 2009), plays a significant role in modulating local carbonate system dynamics ((Thomas et al., 2009; Voynova et al., 2019).). The seasonal TA production, which ranged between 11.7—26.8 mmol m⁻²·d⁻¹ in the spring and summer months and southern North Sea, exhibited a regional TA variability of up to 100 μmol kg⁻¹·, which was attributed to the influence of the extensive sand and mudflats in the Wadden Sea (Voynova et al., 2019).), and to benthic TA production (Brenner et al., 2016). The observed seasonal changes of TA can affect the coastal ocean capacity to absorb carbon from the atmosphere (Burt et al., 2016; Gruber et al., 2019; Li et al., 2024; Schwichtenberg et al., 2020).

The current study focuses on seasonal and inter annual changes in and around the coastal, tidally driven East Frisian Wadden Sea, aiming to identify the sources of TA and DIC responsible for the previously observed seasonal increase in adjacent coastal regions. We conducted seasonal cruises and combined underway FerryBox measurements, carbonate system measurements and nutrient data to characterize the effect of primary production and nutrient cycling on TA generation and carbon dynamics in the East Frisian Wadden Sea. The resultant regional and seasonal distributions of TA and DIC contribute to the elucidation of the potential sources of carbon and TA in this region.

This study offers a detailed analysis of seasonal and inter-annual carbonate system dynamics in the EFWS, a key region within the world's largest intertidal sand and mudflat system (UNESCO World Heritage Centre, n.d.). As an essential component of coastal carbon cycling, and a land-sea junction, this area requires a deeper understanding of the processes influencing TA and DIC. The research focuses on seasonal and regional variations, and particularly on the drivers of TA production in spring-summer. By examining changes in TA, DIC, and other biogeochemical parameters, this study identifies key mechanisms affecting carbonate chemistry, including calcium carbonate (CaCO₃) dissolution and formation, photosynthesis and respiration. Our findings highlight the complex interactions among these factors, emphasizing the need for a comprehensive understanding of regional and seasonal variations to better assess the role of coastal systems in carbon cycling, storage, and climate regulation. Moreover, observed TA and DIC distributions provide valuable insights into potential carbon and TA sources within this dynamic environment.

2 Material and Methods

2.1 Study Side

85

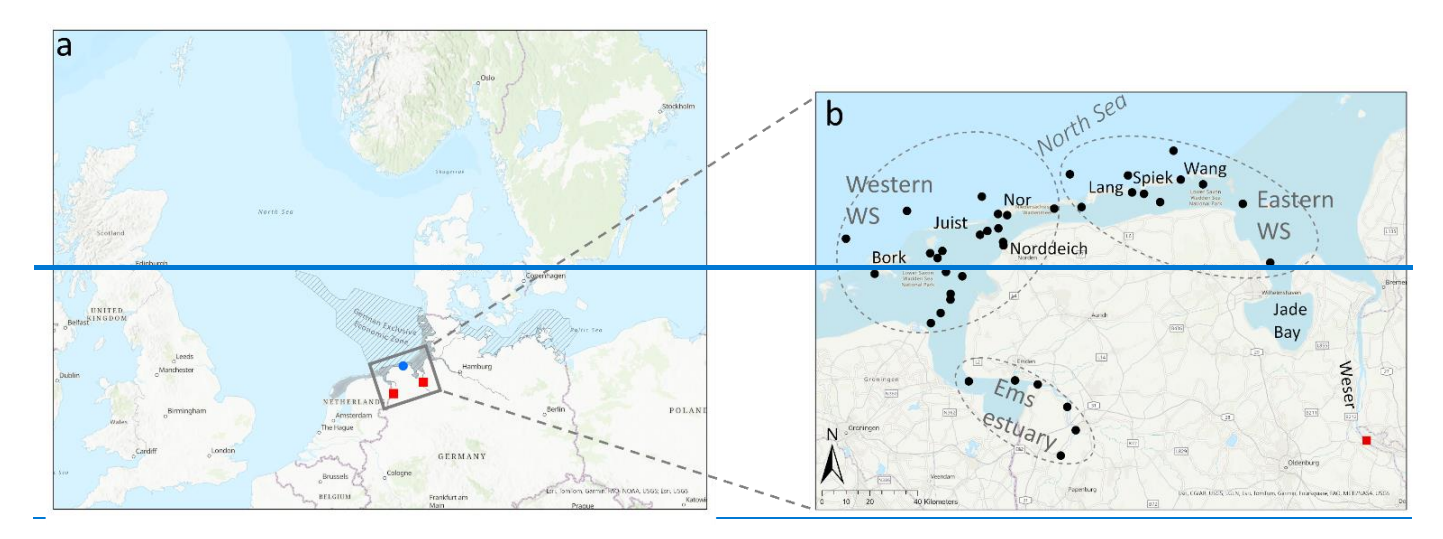
90

The German Bight region is bordered by Germany, Denmark and the Netherlands, and is situated in the southeastern corner of the North Sea (Fig. 1a). The East Frisian Wadden Sea (EFWS) is one of the shallowest regions of the German Bight,

characterized by a series of barrier islands, (Fig. 1b), each 5—_17 km long and 2—_3 km wide (Staneva et al. 2009)...). The system is an intertidal region, influenced by semidiurnal tides with a tidal range from approximately 2.2—_2.8 m (Grunwald et al. 2009; Staneva et al. 2009) and up to ~ 3.5 m in the Elbe River mouth (Staneva et al. 2009).

We separated the study area in two regions (Western WS & Eastern WS; Fig. 1b) due to the differences in the tidal dynamics and hydrodynamic properties (Herrling and Winter, 2015), which drive the area's carbon dynamics, sediment transport, and overall ecological functioning. The tidal range increases from 2.4 m at Borkum to 3.0 m at Wangerooge, with the Eastern region experiencing stronger tidal influences (Herrling and Winter, 2015). In the Langeoog basin, wind effects cause the largest relative increase in residual discharge, while Norderney experiences the largest absolute increase in water flux. Westerly winds influence residual circulation and sediment transport differently in each region. The flow dynamics between the basins of Baltrum and Langeoog are interconnected, whereas the flow regime between Borkum and Norderney is more independent from the dominant circulation patterns and inter-basin exchange (Herrling and Winter, 2015).

)-Seasonal cruises were completed in the Wadden Sea (WS) and North Sea around the East Frisian Islands (and the Ems River estuary-on) with the research vessel (RV) "Burchana" (Lower Saxony department of water management, coastal protection, and nature protection (NLWKN; Fig. 1). The cruises in July 2021 and October 2021 were carried out only in the intertidal East Frisian WS. Later cruises were extended to the Ems River Estuary, from the weir in Herbrum to the island of Borkum (Bork, Fig. 1b); the Ems drains a catchment area of about 12,600 km² (Talke and De Swart 2006). Samples were taken following the salinity gradient up to Weener with a salinity of ~ 0 in the Ems River estuary 1b). The July 2021 and October 2021 cruises focused exclusively on the intertidal mudflats of the EFWS. The RV Burchana, with a draft of 1.3 meters, allowed sea water sampling even during low tide, providing the opportunity to collect samples at various tidal stages. Sampling took place during daylight hours, typically starting in the morning at low tide and continuing throughout the day, with no nighttime samples collected. Both shallow intertidal areas (accessible due to the vessel's low draft) and deeper subtidal channels were sampled to ensure comprehensive spatial coverage.



Later cruises extended into the Ems River Estuary, from the island of Borkum (Bork, Fig. 1b) to Weener (53°09'55.4"N 7°20'39.9"E), a town located upstream the Ems River. These additional data from the Ems River will be presented in a subsequent paper.

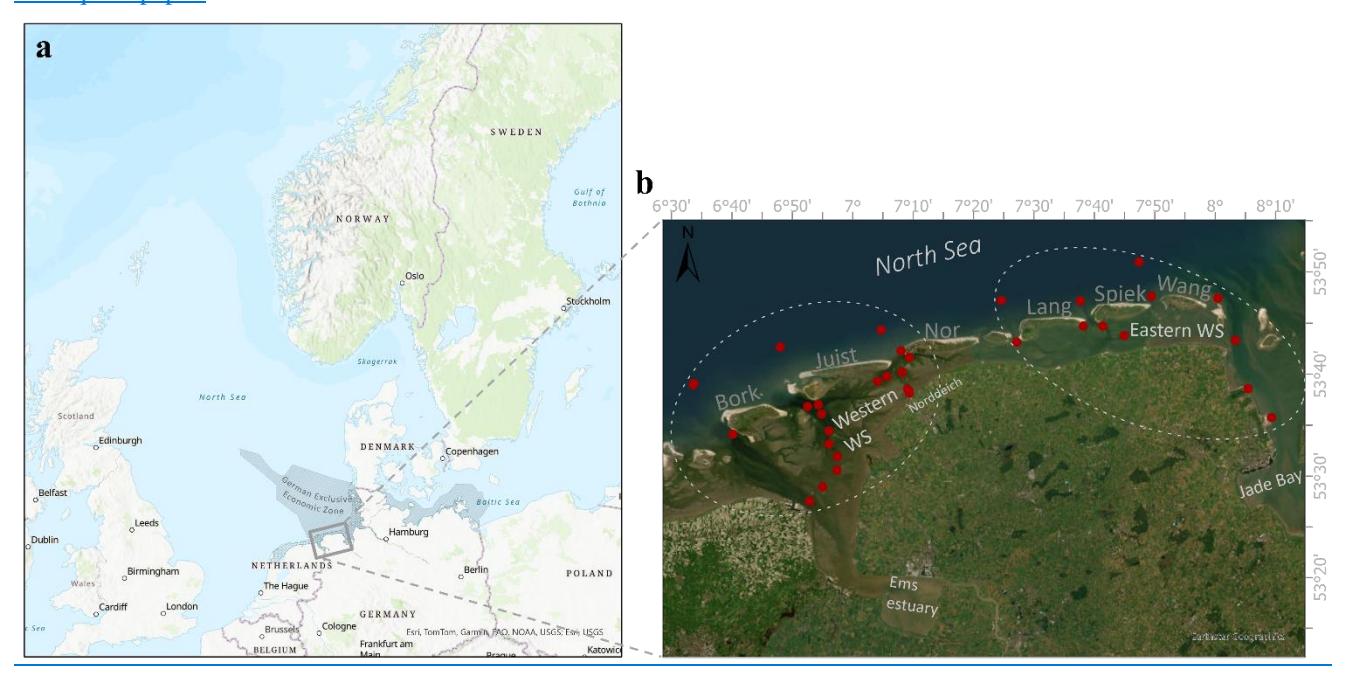


Figure 4:1: Study area, (a) The German Wadden Sea (=WS), (shown in grey) with the German Exclusive Economic Zone (hatched region) and the East Frisian WSEFWS region (grey box). (b) Zoom into the East Frisian WSEFWS, showing the sampling stations (blackred dots) in the different regions in the East Frisian WS (Western WS and Eastern WS) considered in this study. The different Islands are labeledlabelled with their the first few letters of their names (Bork= Borkum, Juist, Nor= Norderney, Lang= Langeoog, Spiek= Spiekeroog, Wang= Wangeoog). The red squares show the inflow of the Ems and Wester Rivers into their estuaries. The blue point shows the location of the sluice in Neuharlingersiel. The map in this Figure was generated using ArcGIS. Data sources: (a) Esri, TomTom, Garmin, FAO, NOAA, USGS; (b) Earthstar Geographics. © 2024 Julia Meyer.

130 **2.2 FerryBox measurements**

135

A FerryBox system (4H-JENA engineering GmbH, Jena, Germany) was operated during all cruises of on board the *RV Burchana* (NLWKN), measuring the following parameters every minute: temperature (SBE38, Sea-Bird Scientific), salinity (SBE45, Sea-Bird Scientific), dissolved oxygen (DO) (Optode 4835, Aanderaa, Bergen, Norway), chlorophyll fluorescence to estimate chlorophyll a concentrations (AlgaeOnlineAnalyser, bbe moldaenke), pH (electrode, Xylem), measured on total scale) and turbidity (Solitax inline SC, Hach Lange) and). The pH electrode was calibrated using standard DuraCal buffer solutions at pH 7 and pH 10 (Hamilton Company, USA). The partial pressure of CO₂ (pCO₂) (was measured using a sensor (HydroC CO₂-FT, 4H-JENA engineering), attached to the flow-through system of the FerryBox. The data were corrected using the data processing manual of 4H - Jena engineeringEngineering GmbH (4H Jena, 2021).). Regions near the ports were excluded in all datasets, to remove any influence of from the ship in-port, or from the cleaning cycles.

140 2.3 Discrete samples

155

160

165

170

Chlorophyll a was not measured in March and May 2022 in the whole Ems River estuary, due to interference by turbidity in the hyper turbid Ems River estuary (Schulz et al. 2022). Samples for 100 Winkler titration (dissolved oxygen), nutrients, salinity and turbidity were collected from each cruise from October 2021 and until July 2022 to crosscheck the measurements of the FerryBox. Therefore, dissolved 2.3 Discrete samples

Dissolved oxygen (DO) samples were collected on the last day of each cruise from October 2021 until July 2022 by filling Biological Oxygen Demand (BOD) bottles from the FerryBox outflow for at least one minute with water overflow to remove 105 any bubbles. Three replicates at each station were collected and 2 mL of each manganese sulfate and alkali iodide azide reagents were pipetted in each sample just below underway were treated according to the surface of the liquid, with care that no bubbles were introduced. Each BOD bottle was carefully stoppered and mixed by inverting the sample several times. All DO samples were standard Winkler method and measured within 24 hours of collection in the lab withusing a Metrohm 870 KF Titrino Plus. The Winkler titrations were used to correct the FerryBox dissolved oxygen measurements from the seasonal cruises. A single regression equation for the Winkler oxygentitrations and the FerryBox data was used to apply a salinity and temperature dissolved oxygen correction of the entire data set (y= 1.17x—_31.89, R²= 0.98, n= 46). In addition, the apparent oxygen utilization (AOU) was calculated from allusing the corrected oxygen measurements, which is defined as: as according

$$AOU = O_2' - O_2$$
 (1)
 $AOU = O_2' - O_2$ (1)

Where $O_2 O_2$ is the expected oxygen at in μ mol L^{-1} at equilibrium with the atmosphere, at given the measured temperature and salinity according to Grasshoff et al., (1999), and in μ mol L^{-1} , whereas O_2 is the oxygen concentration measured by the FerryBox optode 4835, in μ mol L^{-1} .

Duran bottles (~ 300 mL) were filled with sample water during all seasonal sampling cruises using the FerryBox outflow to measure turbidity and salinity in the laboratory. The samples were capped tightly and measured within a few days of collection in the laboratory. Turbidity in the lab was measured with a Hach Turbidimeter 2100. Salinity was measured withusing an OPTIMARE High Precision Salinometer (Optimare Systems GmbH, Bremerhaven, Germany). The) and turbidity and salinity lab measurements were used to quality control the FerryBox measurements was measured using a Hach 2100 turbidimeter. The nutrient waterNutrient samples were taken directly with the water sampler on board of the RV Burchana collected at each station (Fig. 1)-using the onboard water sampler. A sample volume of 250 mLml was filtered usingthrough pre-combusted GF/F filters, and the samples were collected in clean centrifugecentrifuged tubes, which was frozen and stored at -20 °C. NitriteThe concentrations of nitrite (NO₂⁻), nitrate (NO₃⁻) ammonium (NH₄⁺) and silicate (SiO₂) concentrations were also measured viausing a MicroMac analyzeranalyser from SYSTEA (Anagni (FR), Italy). The system is located on board of the RV Burchana (NLWKN), inducing, which induces a colorcolour reaction, is coupled with a photometer (NO₂⁻, NO₃⁻, NO₂⁻, SiO₂) and a fluorometer (NH₄⁺), using a one-point calibration. Distilled ultrapure water was used for the automatically aspirated dilutions. NO₃⁻ was determined with sulfanilamide and N- (1- Naphthyl)ethylenediamine, NH₄⁺ with orthophthalaldehyde and

NO₂⁻ with diethylenetriaminepentaacetic acid and automatic UV reduction (Luitjens, 2019). <u>Silicium reacts with molybdic</u> acid in acidic media to form yellow heteropoly acids. Upon reduction in a strongly acidic solution, a deep blue reaction product, referred to as "silicomolybdic blue," is obtained (Luitjens, 2019).

Water samples for TA and DIC were collected in 300 mL BOD bottles at all stations using the FerryBox outflow according to the Standard Operating Procedure (SOP) for carbonate system sample collection (Dickson et al. 2007)...). The samples were poisoned with saturated mercury chloride solution in order to stop any biological activity. The samples were stored in the dark, at room temperature, and measured in the laboratory with a VINDTA 3C (MARIANDA, Kiel, Germany), and calibrated using certified reference material (CRM) (Dickson et al. 2003)...). The results within this study were plotted with R Project (ggplot package) and maps were created with ArcGIS Pro. In addition, the saturation state of calcite (\(\Omegacol\)\(\Omeg

2.4 Temperature normalized pCO2 estimation

180

190

195

Changes in temperature influence the pCO₂ value of surface waters by controlling the thermodynamic equilibrium of the inorganic carbon system (Takahashi et al. 1993) and thus is affected by seasonal changes (Takahashi et al. 2002). To calculate the thermal component (pCO_{2-therm}) of the observed pCO_{2-therm}) the equation of Takahashi et al. (1993) was used:

$$pCO_{\frac{T_{\text{therm}}}{2}} = pCO_{\frac{T_{\text{obs} Mean}}{2}} * \exp[0.0423 * (T_{\text{obs}} - T_{\text{Mean}})]$$
(2)

*p*CO_{2-obs Mean} is the annual mean *p*CO₂-observed, and T_{Mean} is the annual mean surface temperature over the year. The biological component was also calculated (Takahashi et al. 1993; Kitidis et al. 2019):

$$pCO_{\frac{2}{\text{bio}}} = pCO_{\frac{2}{\text{chio}}} * \exp[0.0423 * (T_{\text{Mean}} - T_{\text{obs}})]$$
(3)

2.4 [TA-DIC] as a proxy for Biogeochemical Processes

[TA-DIC] is a good proxy for biogeochemical processes such as CaCO₃ precipitation / formation, photosynthesis, respiration and therefore CO₂ uptake and release, even in coastal oceans (Xue and Cai, 2020). The parameter is independent of ocean mixing and not sensitive to temperature and pressure changes, and this makes it a good tracer for larger-scale oceanographic studies, and suitable for seasonal observations of biogeochemical processes and carbonate dynamics of an ecosystem. In addition, it is assumed that [TA-DIC], can better reflect variations of [CO₃²⁻] compared to the ratio of TA and DIC (Xue et al., 2017).

The difference between TA and DIC is often expressed as:

$$200 \quad [TA - DIC] = TA - DIC \tag{2}$$

However, [TA–DIC] should not be used at low salinity (e.g. <20) and when [TA–DIC] is < ~50 μmol kg⁻¹, where the relationships of [TA–DIC] with pH and/or ocean acidification are nonlinear, these low values also occur in oxygen minimum zones (Xue and Cai 2020).

2.5 Calculations of estuarine DIC and TA contributions

215

The separation of the different regions within the East Frisian WS allows to use to different riverine endmember for each defined region. For the Western WS we used the measured DIC values of the Ems River estuary with the lowest measured salinity to estimate DIC_{river} in March, May and July 2022. In July 2021 we used the results of discrete samples at the Herbrum 150 Wehr, taken in August 2021 and in October 2021, the discrete samples from the end of October 2021 (Table 1). For the Eastern WS, the Weser River (Fig. 1, marked in red) was used to calculate an average of DIC_{river} (Table 1). Therefore, the Weser River was sampled in August 2021, October 2021 and April 2022.

Table 1: DIC_{river}, DIC_{ocean}, S_{ocean}, TA_{river}To estimate the contributions of estuarine DIC and TA in the Western and Eastern EFWS, we used DIC measurements from the lowest salinity station in the Estuary where the Ems enters the Wadden Sea as endmembers for our mixing model. The stations chosen for these measurements were in areas of low salinity within the estuary, with considerable influence of freshwater (Table 1). These values (DIC_{estuary}; TA_{estuary}) were used to calculate the DIC_{mixing w/R} and TA_{mixing w/R} (equation 3; 4) for the different regions.

Table 1: DICestuary, DICNorthSea, SNorthSea, TAestuary and TAestuary and TAestuary used for the calculation of the seasonal DICmixing w/R concentrations of each season.

Season and Region	DICriver	DICocean	Socean	TAriver	TAocean
	<u>DIC</u> NorthSea	DIC _{estuary}	S <u>NorthSea</u>	TA _{NorthSea}	TA estuary
July 2021					
Eastern WS	2701.7	2119.8	32.05	2435.7	2273.7
Western WS	2491.9	2152.5	31. 50 - <u>79</u>	2541.1	2365.2
	2144.07	<u>2261.20</u>		2273.70	<u>2465.12</u>
October 2021					
Eastern WS	2577.2	2188.5	30.63	2467.9	2369.3
Western WS	2418.7	2176.4	30.97	2321.6	2378.7
	<u>2188.46</u>	2224.90		<u>2369.27</u>	<u>2411.68</u>
March 2022			31.47		
Eastern WS	2647.2	2205.7	29.92	2205.7	1824.8
Western WS	2785.2	2187.9		2187.9	2622.9
	2205.66	2238.05		2338.37	2318.90
May 2022			32.13		
Eastern WS	2647.2	2119.9	31.6	1824.8	2332.5
Western WS	2864.1	2084.5		2722.5	2351.2
	<u>2199.86</u>	2205.52		2332.49	<u>2447.76</u>
July 2022			31.78		
Eastern WS	2647.2	2144.4	32.03	1824.2	2356.6
Western WS	2929.3	2173.9		2853.7	2396.6
	<u>2144.41</u>	2310.22		2356.59	2489.56

The influence of the riverine input can affect the carbon dynamics, especially in a shelf sea such as the North Sea. In this study, DIC_{NorthSea} (and TA_{NorthSea}) refers to the DIC (and TA) values at the station (CAR S 076) located farthest from land behind Spiekeroog and Wangeoog (Fig. 1b), which we used the equation as our marine endmember, as it is situated farthest offshore of the Ems and experiences the highest salinity (S_{NorthSea}) levels during almost each season. The DIC_{NorthSea} and TA_{NorthSea} endmembers applied for each season are shown in Table 1.

Starting with these endmembers, we used the equations of (Jiang et al. (2008) and ;-Joesoef et al. (2015) to calculate DIC mixing with these endmembers, we used the equations of (Jiang et al. (2008) and ;-Joesoef et al. (2015) to calculate DIC mixing with these endmembers, we used the equations of (Jiang et al. (2008) and ;-Joesoef et al. (2015) to calculate DIC mixing with these endmembers, we used the equations of (Jiang et al. (2008) and ;-Joesoef et al. (2015) to calculate DIC mixing with these endmembers, we used the equations of (Jiang et al. (2008) and ;-Joesoef et al. (2015) to calculate DIC mixing with these endmembers, we used the equations of (Jiang et al. (2008) and ;-Joesoef et al. (2015) to calculate DIC mixing with these endmembers, we used the equations of (Jiang et al. (2008) and ;-Joesoef et al. (2015) to calculate DIC mixing with the equations of (Jiang et al. (2008) and ;-Joesoef et al. (2015) to calculate DIC mixing with the equations of (Jiang et al. (2008) and ;-Joesoef et al. (2015) to calculate DIC mixing with the equations of (Jiang et al. (2008) and ;-Joesoef et al. (2015) to calculate DIC mixing with the equations of (Jiang et al. (2008) and ;-Joesoef et al. (2015) to calculate DIC mixing with the equation of (Jiang et al. (2008) and ;-Joesoef et al. (2015) to calculate DIC mixing with the equation of (Jiang et al. (2008) and ;-Joesoef et al. (2015) to calculate DIC mixing with the equation of (Jiang et al. (2008) and ;-Joesoef et al. (2015) to calculate DIC mixing with the equation of (Jiang et al. (2008) and ;-Joesoef et al. (2015) to calculate DIC mixing with the equation of (Jiang et al. (2008) and ;-Joesoef et al. (2015) to calculate DIC mixing with the equation of (Jiang et al. (2008) and ;-Joesoef et al. (2015) to calculate DIC mixing with the equation of (Jiang et al. (2015) and ;-Joesoef et al. (2015) to calculate DIC mixing with the equation of (Jiang et al. (2015) and ;-Joesoef et al. (2015

$$DIC_{\text{mixing w/R}} = \frac{S_{\hat{t}}}{S_{\text{ocean}}} + DIC_{\text{ocean}} + (1 - \frac{S_{\hat{t}}}{S_{\text{ocean}}}) * DIC_{\text{river}}$$

$$DIC_{\text{NorthSea}} + (1 - \frac{S_{\hat{t}}}{S_{\text{NorthSea}}}) * DIC_{\text{estuary}}$$
(3)

which is the DIC concentration after mixing of the DIC concentration of the nearshore regions (DIC_{ocean}) and the DIC concentration of the riverine endmember Weser and Ems (DIC_{river}). The S_i and S_{ocean} are the salinity concentrations of the station i and the North Sea endmember (nearshore regions) with the seasonal highest salinity measured in the Western and

230 Eastern regions.

 $\Delta T \Lambda_{excess} = T \Lambda_{I-} - T \Lambda_{mixing w/R}$

220

$$TA_{\text{mixing w/R}} = \frac{S_i}{S_{\text{NorthSea}}} * TA_{\text{NorthSea}} + (1 - \frac{S_i}{S_{\text{NorthSea}}}) * TA_{\text{estuary}}$$
(4)

where S_i represents the salinity at each related station *i*. The ratio $\frac{S_i}{S_{NorthSea}}$ normalizes the influence of the salinity at the specific station by the salinity of the North Sea ($S_{NorthSea}$).

In Addition addition, the ΔDIC_{excess} was calculated to estimate the contribution due to riverine input in the different regions. Therefore, the equation of (Jiang et al., 2008; (Van Dam et al., 2018; Jiang et al., 2008)) was used:

$$\Delta DIC_{\text{excess}} = \frac{DIC_{+}}{DIC_{i}} - DIC_{\text{mixing w/R}}$$
(5)

This equation includes the measured DIC concentrations of the related station i and the DIC_{mixing w/R}.of equation $4\underline{3}$. $\Delta TA_{\text{mixing w/R}}$.and $\Delta TA_{\text{excess}}$ were calculated the same way with the measured TA of each station using the $\overline{TA_{\text{river}}}$, $\overline{TA_{\text{ocean}}}$ concentrations $\overline{TA_{\text{estuary}}}$, $\overline{TA_{\text{NorthSea values}}}$ (Table 1):

240
$$\Delta TA_{\text{excess}} = TA_i - TA_{\text{mixing w/R}}$$

$$= \frac{S_{\ddagger}}{S_{\text{ocean}}} + TA_{\text{ocean}} + (1 - \frac{S_{\ddagger}}{S_{\text{ocean}}}) * TA_{\text{river}}$$
(6)

ΔDIC_{excess} and ΔTA_{excess} concentrations were calculated to remove the mixing effect of the rivers water masses from the estuary outflow with the sea. The North Sea, as the coastal region of the East Frisian WSEFWS is closely connected to the land and the rivers are usually supersaturated with CO₂compared to the atmosphere (Joesoef et al. 2015). A ΔDIC_{excess} value of approximately zero means that the DIC is not different than what would be expected upon from mixing between the ocean North Sea and river estuarine outflow waters. Negative values of ΔDIC_{excess} confirmindicate that the DIC consumption exceeded production in this area, which reduces DIC or, equivalently increases ΔTA_{excess}. Positive values of ΔTA_{excess} suggests higher

values than expected based on mixing alone, indicating other additional TA sources are present, caused for instance by biogeochemical processes such as CaCO₃-dissolution and respirationTA sources.

Therefore, during high-productive seasons, the-primary production will increase TA and decrease DIC, while consuming CO₂ and nutrients (Xue and Cai, 2020). The uptake of NO₃-willcan increase and TA, while the uptake of NH₄+willcan decrease TA in an ecosystem (Brewer and Goldman, 1976; Wolf-Gladrow et al., 2007). The production of 1 mol organic matter ((CH₂O)₁₀₆(NH₃)₁₆H₃PO₄) will generally increase TA by 17 mol TA (ΔTA_P) and decrease DIC by 106 mol and will change the TA and DIC concentrations (Chen, 1978). Therefore Consequently, ΔTA_P is used to calculate the expected amount of TA produced and decrease DIC by primary producers, according to the equation of ΔTA_{bio} from (Xue and Cai 2020), which was modified using the calculated ΔDIC_{excess}:

$$\Delta TA_{\mu} = -17/106 * \Delta DIC_{excess}$$

$$However, it \Delta TA_{\mu} = -17/106 * \Delta DIC_{excess}$$
(8)

260 _____(7)

250

255

It is important to note, that the calculation of ΔTA_P is an overestimation assuming the measured TA is resulting only due to modulated by photosynthesis (NO₃--- fueled) or respiration. Additionally, such that the East Frisian WS is also influenced by tidal variability and presence of other riverine inputs from land for instance Rhine River or Elbe Rivernon-photosynthetic DIC sinks will cause ΔTA_P to be overestimated.

265 3 Results

270

275

3.1 Intertidal East Frisian Wadden Sea

3.1.1 Regional and seasonal variation in the EFWS

In July 2021, salinities were lowest on the route from Norddeich harborharbour to Norderney (25.212), and in the intertidal region around Norderney (Table 2; Fig. 2S1) in the Western WS. In summer 2022, the salinity on July 12 (31.16 - 32.03) increased by 2 - 3 salinity units compared to July 11 (28.28 - 29.43) in the Eastern WS (Table 2; Fig. 2S1). This indicates that during July 2022 cruise, there was a change in salinity range between the first and second leg of the cruise (in roughly the same region). A possible reason for these salinity differences could be the Neuharlingersiel sluice opening in the early morning of July 11, 2022, which could have influenced the salinity on this day. The turbidity in October 2021 showed a completely different pattern compared to all other seasons, with values from 96.08 – 306.46 NTU (Fig. 2S1), caused by rougher weather conditions during the campaign. However, slight regional differences in turbidity were measured, for instance in the Jade Bay in March 2022, as well as in the intertidal WS near Juist (Fig. 2).

A land to sea gradient was observed in pH in October 2021 (Fig. S2), which varied from 7.6 to 8.1 (Table 2). Higher values were measured in the North Sea regions (behind Juist, Norderney, Langeoog), whereas the lower values were measured closer

to the mainland. Regional differences with maximum pH values of > 8 in the higher salinity waters were measured during all seasons (Fig. S2; Table 2), with pH > 8 in the Western WS, in front of Norderney in May 2022.

Table 2: Overview of the different measured parameters: Temperature (°C), Salinity, pH, oxygen (% saturation), AOU (μ mol L-1), Chlorophyll a (Chl a in μ g L-1), pCO_{2 obs} (μ atm) and Aragonite Calcite saturation Ω cal of all seasonal samplings. The given values of the Calcite saturation state (Ω cal) are separated in the low saline Ems Estuary and the East Frisian Wadden Sea (Eastern WS, Western WS) in high salinity waters EFWS.

Parameter	July 2021	October 2021	March 2022	May 2022	July 2022
Temperature (°C)	18.59 − 23.15 * [±]	$12.66 - 16.57 \stackrel{*}{=}{}^{1}$	$3.89 - 6.47 \stackrel{*2}{=}$	9.65 – 18.19 ≛ ²	17.36 – 21. 88* ² <u>04</u>
Salinity	$25.21 - 32.33^{\pm 4}$	25.21— <u>_</u> 31.32 <u>*</u> [‡]	$\frac{0.2518.32}{97*^2} - 31.$	0.36 23.59 − 32.28 <u>*</u> 2	$\frac{123}{35} - 32.04 \stackrel{*}{=} 2$
pH	$7.71 - 8.16^{*1}$	$7.64 - 8.13^{\pm 1}$	$7.3366 - 8.13^{2}$	7.2595 - 8.56*255	$7.3071 - 8.08 \pm 2$
Oxygen (% sat)	109.7 ± 9.5 * [±]	$100.9 \pm 5.3 \stackrel{*}{=} 1$			
East Frisian	_	_			
Wadden Sea:			$\frac{104.9}{105.5} \pm 3$.	$\frac{129.6 \pm 15.3 *^{4}}{}$	$\frac{101.2}{102.4} \pm 5.9*$
Ems Estuary:			3* 1	$45.5 \pm 20.8 \underline{132.9}$	+
			77.8 ± 10.6	<u>± 13.0</u>	65.6 ± 25.42
AOU (µmol L-1)	-22.7 ± 22.2**	-2.3 ± 14.4 **			
East Frisian	_	_			
Wadden Sea:			-15.9 _	$-39.1 \pm 97.2 *^{1}$	$\frac{-2.9 \pm 14.2 *^{1}}{2}$
Ems Estuary:			$17.5 \pm 10.9 ^{*1}$	$\frac{164.2 \pm 64.2}{}$	$91.6 \pm 70.2_{-}$
			85.2 ± 41.30	88.9 ± 33.9	5.3 ± 12.4
Chl a (µg L-1)	$25.6 \pm 12.9^{\pm 1}$	16.9 ± 8.9 ^{±‡}	$13.34 \pm 6.3*25$	$42.0 \pm 27.9 \pm 252.1$	$23.2 \pm 19.3 \stackrel{*2}{=}$
				<u>± 29.4</u>	
pCO _{2 obs} (µatm)		$521.6 \pm 72.2^{*4}$			536.0 ± 116.5 **
East Frisian		_			2237.9 ± 1109.1
Wadden Sea:	_		4 85.6 ±	$319.4 \pm 202.9 * ^{4}$	
Ems Estuary:	_		73 468.2**	$\frac{1521.5 \pm 1318.42}{}$	
			2306.9 ± 534.1	69.0 ± 63.7	
			<u>± 54.5</u>		
Ωcal	3.8 ± 0.9 ≛ ‡	3.21 ± 0.6**	$2.65 \pm 0.3 \pm 1$	5.2 ± 1.1 *1	3.87 ± 0.4
East Frisian	_	_	0.9 ± 0.64	1.1 ± 0.7	1.9 ± 0.8
Wadden Sea:					
Ems Estuary:					

^{**}Cruises, containing the Western and Eastern part of the East Frisian Wadden Sea (Western WS & Eastern WS)

280

^{*2} Cruises, which covered not only the intertidal regions, but also the Ems River Estuary

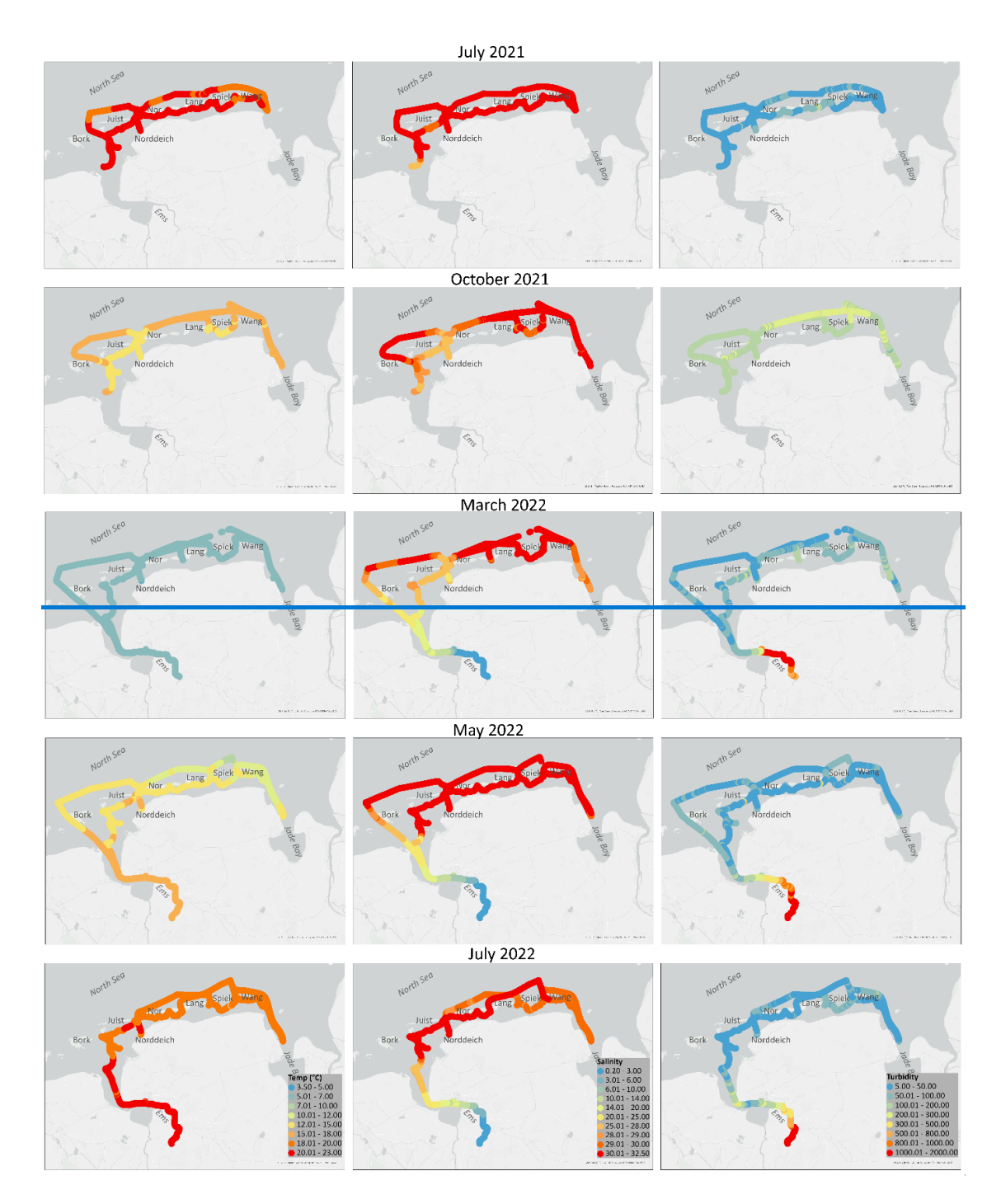


Figure 2: Results of all seasonal cruises from July 2021, October 2021, March 2022, May 2022 and July 2022 measured with the FerryBox. Temperature (°C), Salinity (PSU) and Turbidity (FNU). The map in this Figure was generated using ArcGIS. Data sources: LGLN, Esri, TomTom, Garmin, Foursquare, FAO, METI/NASA, USGS. © 2024 Julia Meyer.

A land to sea gradient was observed in pH in October 2021 (Fig. 3), which varied from 7.64 to 8.13 (Table 2). Higher values were measured in the North Sea regions (behind Juist, Norderney, Langeoog), whereas the lower values were measured closer to the mainland. The highest pH values were measured in May 2022 (Fig. 3; Table 2) with the highest variability and pH > 8 in the Western region, in front of Norderney. Regional differences with maximum pH values of > 8 in the higher salinity intertidal waters were measured during all seasons (Fig. 3).

The concentrations of chlorophyll a were observed in May 2022—was, displaying the highestmost substantial fluctuations (Table 2; Fig. 3) overall, with the greatest variance (Table 2), and), especially, in the Western part of the East Frisian WS from Norderney to Borkum (up to 151.7—µg_µg_L⁻¹) (Fig. 3_S2). In July 2021, the highest chlorophyll a-measurements (up to 74.7 µgµg_L⁻¹) were detected in the intertidal region from underway between Norderney to Spiekeroog (Table 2; Fig. 3), whereas lower values (down to 2.8 µg L⁻¹) were observed in the North Sea regions of the transects. S2). A similar pattern can be seen for July 2022 in the intertidal zone (Fig. 3_S2), however no measurements of the transect from Norderney to Spiekeroog isare available for chlorophyll a. This is also the case for October 2021 within the intertidal zone transects from Norderney to Wangeoog (Fig. 3_S2).

A similar seasonal variability was observed for the oxygen (Table 2; Fig. 3). In July 2021 the measured oxygen ranged from 72.4—__112.01 in % saturation (Fig. 3_S2), with the highest values in the intertidal area Wadden Sea of Langeoog. The oxygen saturation Oxygen decreased from July 2021 to October 2021, on average by 8.8 ± ± 10.9 % saturation (Table 2; Fig. 3_S2). The lowest oxygen saturation was measured on the transect from Norddeich to Norderney in October (down to ~57 % saturation). Until May 2022, oxygen saturation increased continuously over the year. The highest oxygen saturation (up to ~180 %) % saturation) was measured in May 2022 in the intertidal region of Norderney in the Western WS and around Wangeoog in the Eastern WSEFWS (up to ~152 %) (Table 2; Fig. 3). However, saturations below 100 % were measured in the section from Norddeich harbor to Norderney (down to 84 % saturation) (Fig. 3) % saturation) (Table 2; Fig. S2). Overall, oxygen saturation in the East Frisian WS decreased by a mean value of 28.4 ± ± 16.4 % 230 % saturation from May 2022 to July 2022 (Fig. 3_S2), resulting in slightly lower oxygen saturation in July 2022 compared to the previous year before (Table 2). The oppositeFor the AOU (Table 2), the same inverse picture was also observed for AOU (not shown), with negative values as it became more saturated (> 100 % saturation) (Table 2) obtained. The observed pCO₂ (pCO_{2 obs}) was highest in July 2022 and lowest in May 2022 (down to 141.3 μatm μatm) in the intertidal zone of the Western WS. The average decrease in pCO_{2 obs} was 166.2 ± ± 276.1 μatm μatm from March 2022 to May 2022 (Table 2; Fig. 4) (see also section 3.1.2). S3).

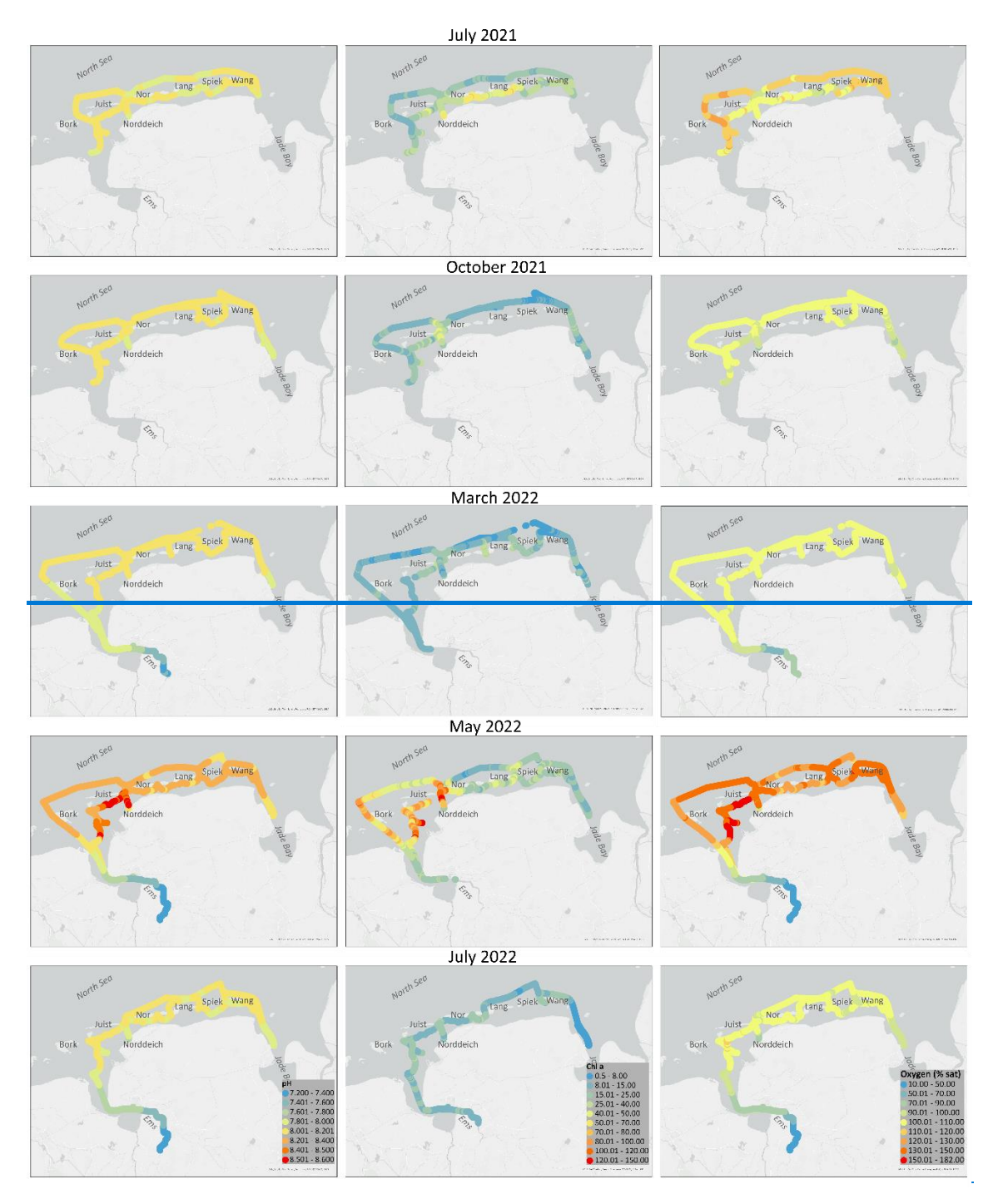
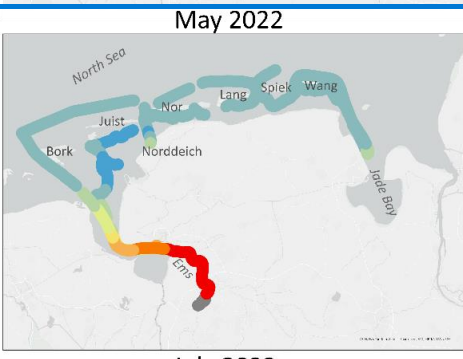


Figure 3: Results of all seasonal cruises from July 2021, October 2021, March 2022, May 2022 and July 2022 measured with the FerryBox, pH, Chlorophyll a (Chl a in µg L¹) and oxygen (% saturation). The map in this Figure was generated using ArcGIS. Data sources: LGLN, Esri, TomTom, Garmin, Foursquare, FAO, METI/NASA, USGS. © 2024 Julia Meyer.

October 2021 North Se⁰ Lang Spiek Wang Juist Norddeich





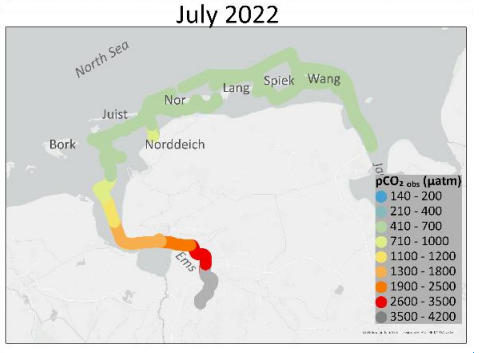


Figure 4: pCO_{2 obs} (µatm) of October 2021, March 2022, May 2022 and July 2022 measured with the FerryBox. The map in this Figure was generated using ArcGIS. Data sources: LGLN, Esri, TomTom, Garmin, Foursquare, FAO, METI/NASA, USGS. © 2024 Julia Meyer.



Figure 5: Calculated Ωcal saturation of the seasonal cruises. July 2021, October 2021, March 2022, May 2022 and July 2022. The map in this Figure was generated using ArcGIS. Data sources: LGLN, Esri, TomTom, Garmin, Foursquare, FAO, METI/NASA, USGS. © 2024 Julia Meyer.

330 The calcite saturation (Ωcal) was calculated (Lewis et al., 1998; Weiss, 1974) for all seasonal cruises to observe where CaCO₃ dissolution and formation may occurs seasonally. During all seasons, Ω cal Ω cal was supersaturated in the intertidal East Frisian WS, ranging from 1.5 - 7.5 (Table 2), but with a pronounced seasonal pattern. Low values (< 2.0) were mainly calculated in October 2021 and March 2022 (Table 2; Fig. 5). Higher, oversaturated Ωcal values (> Higher, supersaturated Ωcal values (> 2.5) were observed during more productive seasons (July 2021, July 2022, May 2022). However, the highest variability of Ω was found in May 2022 with values > 1 in 80 % of the stations and reaching up to 7.52 in the intertidal regionWS of Juist and Borkum (Table 2; Fig. 5). In contrast, in the Ems River estuary, Ωcal saturation decreased (down to < 1) with decreasing salinity during all seasons and was the lowest in March 2022 (Table 2; Fig. 5). S3). In summer (July 2021, July 2022), a decrease of <u>ΩcalΩcal</u> in the <u>East Frisian WSEFWS</u> from West to East <u>can bewas</u> observed, regionally (Fig. 5). The high Ωcal saturation (up to 7.5) in May 2022 in the intertidal zone near Juist and Borkum is outstanding (Fig. 5). These high and oversaturated values can support CaCO₃ formation in this region, and thus calcification of organisms during this highly productive season (May 2022). S3).

3.1 2 Seasonal Shifts in the Dominance of Biological and Thermal Components of pCO2

335

340

345

The thermal effect was removed from pCO_{2 obs} measurements (Fig. 4) to isolate the portion of pCO₂ that can be explained by biological effects (pCO_{2 bio}). The remaining pCO₂ bio reflects the biologically influenced pCO₂, including the effects of biological production and consumption of CO₂, ocean mixing processes, and freshwater inputs (Chierici et al., 2006; Lüger et al., 2004; Tozawa et al., 2022).

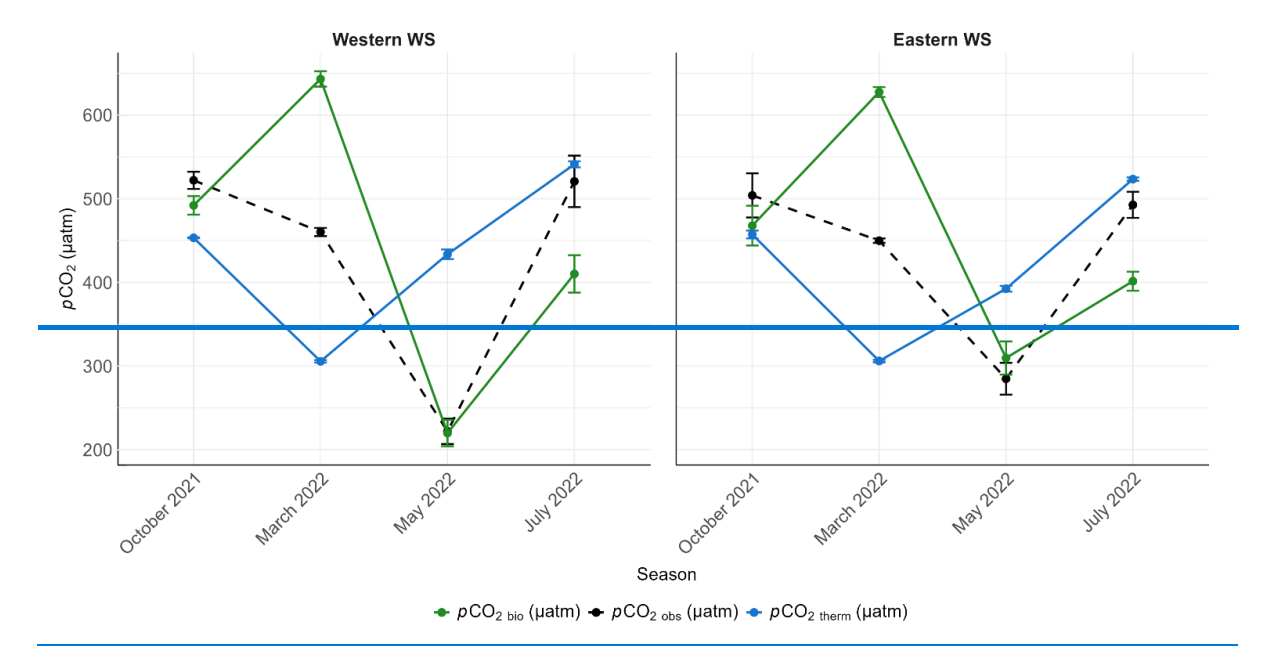


Figure 6: Seasonal thermal component, pCO2 therms, biological component, pCO2 bio and pCO2 observations, pCO the related error bars in the Western and Eastern WS.

The seasonal variability of *p*CO_{2 obs}, *p*CO_{2 therm} and *p*CO_{2 bio} are illustrated in Figure 6. The *p*CO_{2 therm} (453.2 μatm) was slightly lower compared to *p*CO_{2 bio} (492.0 μatm) in October 2021 (Fig. 6), in the Western WS. In March 2022, the biological influence was higher (643.1 μatm) in the Western WS, compared to the *p*CO_{2 therm} indicating both thermal and biological effects influencing the *p*CO_{2 obs} (Fig. 6). By May 2022 the pattern shifted, with substantial low *p*CO_{2 bio} (219.9 μatm), while *p*CO_{2 therm} remained relatively high (433.6 μatm). This predominance of the biological over the thermal component during May contributed to the overall drawdown of *p*CO_{2 obs} (Fig. 6), with similar errors of 15.7 μatm for *p*CO_{2 bio} and 15.2 μatm for *p*CO_{2 obs}. Finally, from May 2022 to July 2022, all *p*CO₂ components increased, with the thermal influence surpassing the biological component. This implies higher thermal influence than biological in the Western WS (Fig. 6).

The Eastern WS exhibits a similar pattern in *p*CO_{2 obs}, *p*CO_{2 therm} and *p*CO_{2 bio} with slightly lower values across all seasons compared the Western WS (Fig. 6). The results demonstrate a clear seasonal shift in the dominance of biological and thermal influences on *p*CO₂. During the colder months (October 2021, March 2022), thermal processes had a more notable impact on *p*CO_{2 obs}. In contrast, biological processes played a more substantial role during the warmer months (May 2022, July 2022), particularly in May, when the biological influence was most pronounced in both regions (Fig. 6).

3.1.33.2 TA and DIC Variability in the EFWS

350

355

360

365

370

375

Large variability in DIC and TA was observed in the East Frisian WS, seasonally but also regionally along the land to sea gradient in the EFWS (Table 3; Fig. 6). Higher 2) with high TA were measured in the intertidal region in summer (July 2021, July 2022) (Fig. 72). In July 2021, TA ranged from ~ 2273 μmol kg⁻¹ in the Jade Bay (Eastern WS) and increased regionally westward (up to ~ 2465 μmol kg⁻¹) to Norderney (Table 3; Fig. 7). Figure 8 also shows the higher 2; Fig. 3a). All measured TA in summer (July 2021, July 2022) in the intertidal region compared to the other seasons. In July 2021, all measured TA values are values were above or slightly below the mixing line with a negative slope (- 24.9 μmol kg⁻¹ per salinity unit) in the intertidal zone of the East Frisian WS (Fig. 8a3a), indicating TA production in this region. In July 2022, lower TA values were measured during the first leg of the cruise when salinities were lower (28 - 29) (Table 3; Fig. 72; Fig. 8a3a), but a similar slope (- 23.3 μmol kg⁻¹ per salinity unit) of the short mixing line in Figure 7a was observed. During the (Fig. 3a). At higher salinity stations in July 2022-cruise, when higher salinities were measured (up to 32), the TA values were similar to those of July 2021-measured the previous summer, with a negative slope of -25.1 μmol kg⁻¹—per salinity unit, slightly above the mixing line, indicating TA production in the intertidal zone (Fig. 8a 3a). The DIC concentrations also showed a similar pattern during both summer cruises (Table 3; Fig. 8b3b), with a negative slopes of - 49.0 μmol kg⁻¹ and - 44.3 μmol kg⁻¹ per salinity unit in July 2021 and in July 2022, respectively, in the Eastern WS.

Table 3: Overview of different the parameters TA (μmol kg⁻¹), DIC (μmol kg⁻¹) and [TA-DIC] (μmol kg⁻¹) of all seasonal samplings in average with the standard deviation.

<u>Parameter</u>	July 2021	October 2021	March 2022	May 2022	July 2022
TA (μmol kg ⁻¹)					
Western WS	2403.4 ± 27.4	2388.6 ± 15.6	2358.6 ± 27.8	2378.9 ± 39.0	2380.2 ± 42.7
Eastern WS	2283.5 ± 10.2	2236.6 ± 5.3	2347.2 ± 11.8	2349.7 ± 9.8	2337.2 ± 35.2

DIC (μmol kg ⁻¹)					
Western WS	2185.8 ± 48.2	2257.1 ± 91.0	2237.7 ± 37.8	2065.5 ± 107.0	2184.4 ± 43.3
Eastern WS	2124.1 ± 10.3	2182.8 ± 18.2	2211.8 ± 20.9	2089.2 ± 38.0	2142.3 ± 27.6
[TA-DIC]					
(µmol kg ⁻¹)					
Western WS	217.55 ± 51.9	150.5 ± 47.1	120.9 ± 30.2	313.3 ± 76.1	196.8 ± 26.7
Eastern WS	159.44 ± 16.4	184.9 ± 19.9	137.9 ± 11.0	260.5 ± 34.7	194.9 ± 21.1

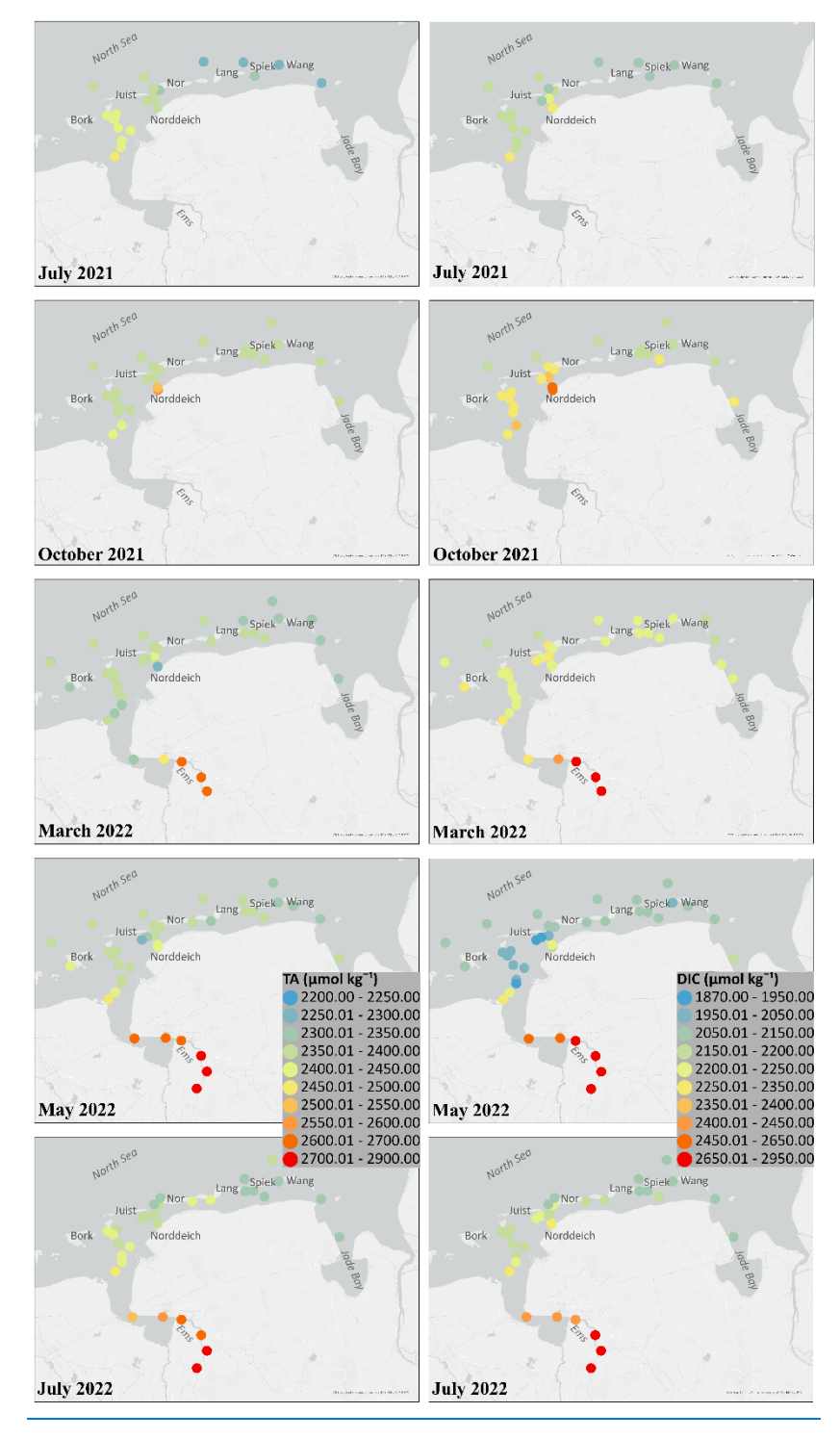


Figure 2: Measured results of TA and DIC of all seasonal cruises of July 2021, October 2021, March 2022, May 2022 and July 2022. All TA and DIC values are in µmol kg ¹¹). The map in this Figure was generated using ArcGIS. Data sources: LGLN, Esri, TomTom, Garmin, Foursquare, FAO, METI/NASA, USGS. © 2024 Julia Meyer.

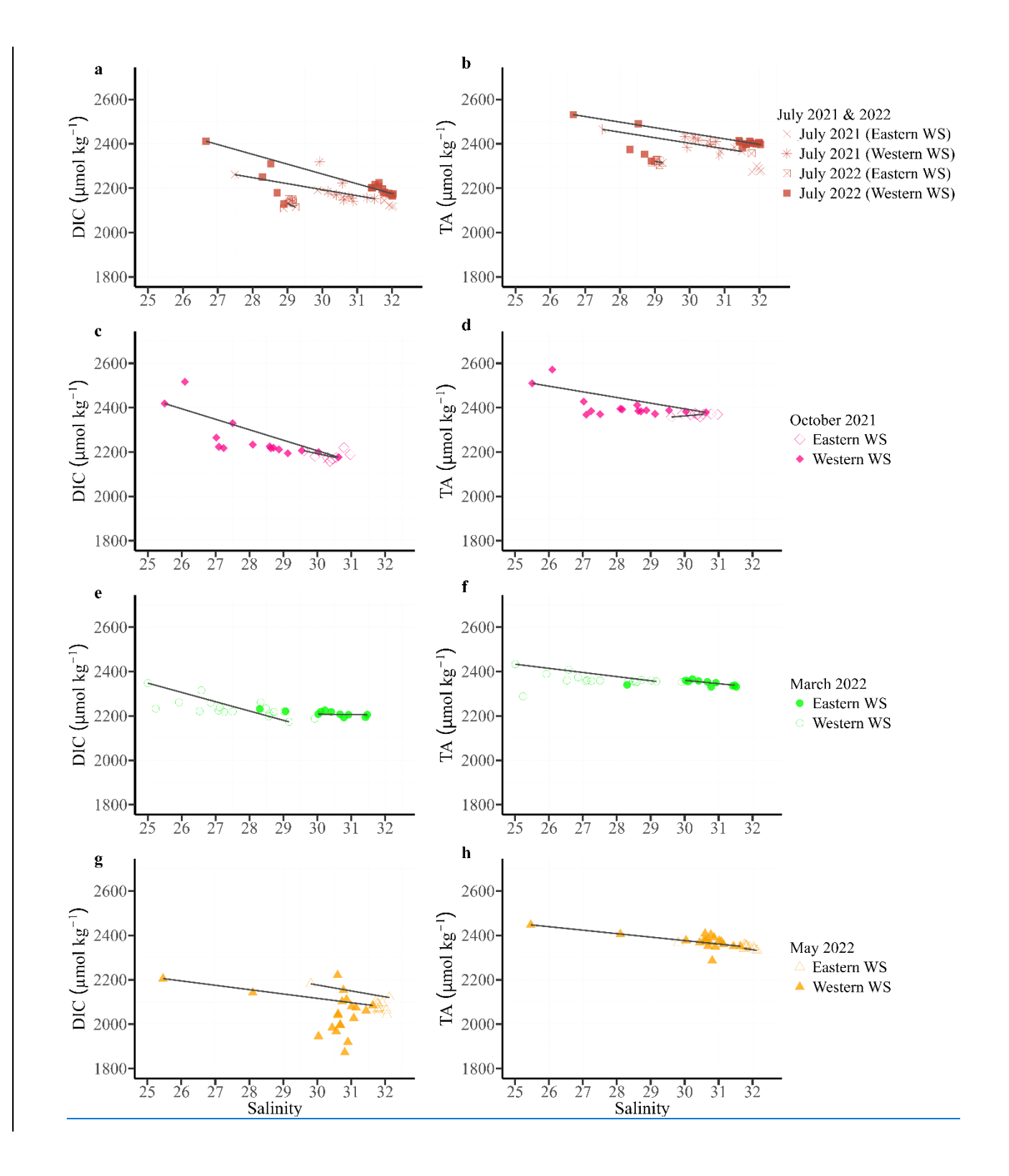


Figure 3: TA (μmol kg⁻¹) and DIC (μmol kg⁻¹) mixing plots, against salinity of July 2021 (a, b), October 2021 (c, d), March 2022 (e, f), May 2022 and July 2022 (a, b) at > 25 salinity, separated by the different regions (Eastern WS-of - 44.3 μmol kg⁻¹ per salinity unit (Fig. 8b)., Western WS) of the EFWS.

In October 2021, the highest TA concentrations were measured at a station near Norddeich (up to 2571 μmol kg⁻¹) in the Western WS (Fig. 7). DIC shows a very similar pattern as for TA during this season (Fig. 7).2). The DIC values reached a maximum of 2516 μmol kg⁻¹ in the intertidal zone in front of Norderney and decreased with increasing longitude to a minimum of 2158 μmol kg⁻¹ (Fig. 72). The mixing plot of TA in October 2021 shows a negative mixing line in the Western WS (- 25.4 μmol kg⁻¹ per salinity unit), whereas the Eastern WS shows an almost linear mixing line with a positive slope of 13.1 μmol kg⁻¹ per salinity unit (Fig. 72; Fig. 8c). The DIC mixing plot (Fig. 8d) shows a3c). A similar picture of TA was observed in the Western WS to TA, with a negative slope (- 46.9 mol kg⁻¹ per salinity unit) (Fig. 3d). In March 2022, lower DIC concentrations (< 2200 μmol kg⁻¹) were measured further offshore behind the islands of Borkum, Juist and Norderney and these increased slightly closer to land (Fig. 7). A few stations in the intertidal zone also recorded higher concentrations than others in the surrounding area. Little variation of TA and DIC in the intertidal zone was found, resulting in an almost linear mixing line of TA and DIC within this region (Fig. 8e, f) in March 2022, which increased slightly closer to land (Fig. 2).

The mean measured TA in the Western WS in May was 2378.9 μmol kg⁻¹ (Table 3, Fig. 2), indicating a slight increase in TA from March to May 2022. Most of the TA values were close to or above the mixing line, with similar negative slopes in the Western (- 15.6 μmol kg⁻¹ per salinity unit) and in the Eastern WS (- 15.3 μmol kg⁻¹ per salinity unit) (Fig. 3g). The lowest DIC values (down to 1872 μmol kg⁻¹) in this study were also measured in the Western WS in spring (Table 3; Fig. 2; Fig. 3h).

3.3 Seasonal Trends in [TA-DIC] and AOU in the EFWS

390

395

400

The relationship between [TA–DIC] and AOU provides valuable insights into the biogeochemical processes that drive carbonate dynamics in coastal systems (Xue and Cai, 2020). A critical threshold for interpreting this relationship is that [TA–DIC] cannot be used when values are < 50 µmol kg⁻¹, as proposed by Xue and Cai (2020). This threshold applied only to one station near Norddeich harbor in October (Fig. 7), so these data were excluded from the seasonal calculations (Table 3).

Figure 4a illustrates the AOU relationship to [TA-DIC] from all stations sampled during various seasons in the Wadden Sea.

The regression analysis highlights a negative correlation, with a slope of -1.416 μmol kg⁻¹ per μmol L⁻¹ of AOU, which is steeper than the Redfield ratio slope (- 123/138 = -0.89), previously proposed by Xue and Cai (2020). In spring, negative AOU values (down to -169 μmol L⁻¹, Fig. 4a) were observed alongside higher [TA-DIC] values (> 200 μmol kg⁻¹; Fig. 4b).

In the summer (2021; 2022), [TA-DIC] values from the Eastern WS are located under the respiration/photosynthesis line (< 200 μmol kg⁻¹; Fig. 4b). In contrast, the measured [TA-DIC] concentrations in the Western WS in summer are > 200 μmol kg⁻¹, above the respiration/photosynthesis fit (Fig. 4b). In July 2022, the salinity in the same region changed by 2 - 3 units from one day (July 11) to another (July 12), where the salinity was higher in the East, showing slightly higher TA

values ($\pm 53.7 \pm 36.7 \,\mu$ mol kg⁻¹) in summer 2022, compared to the previous year (Table 3).

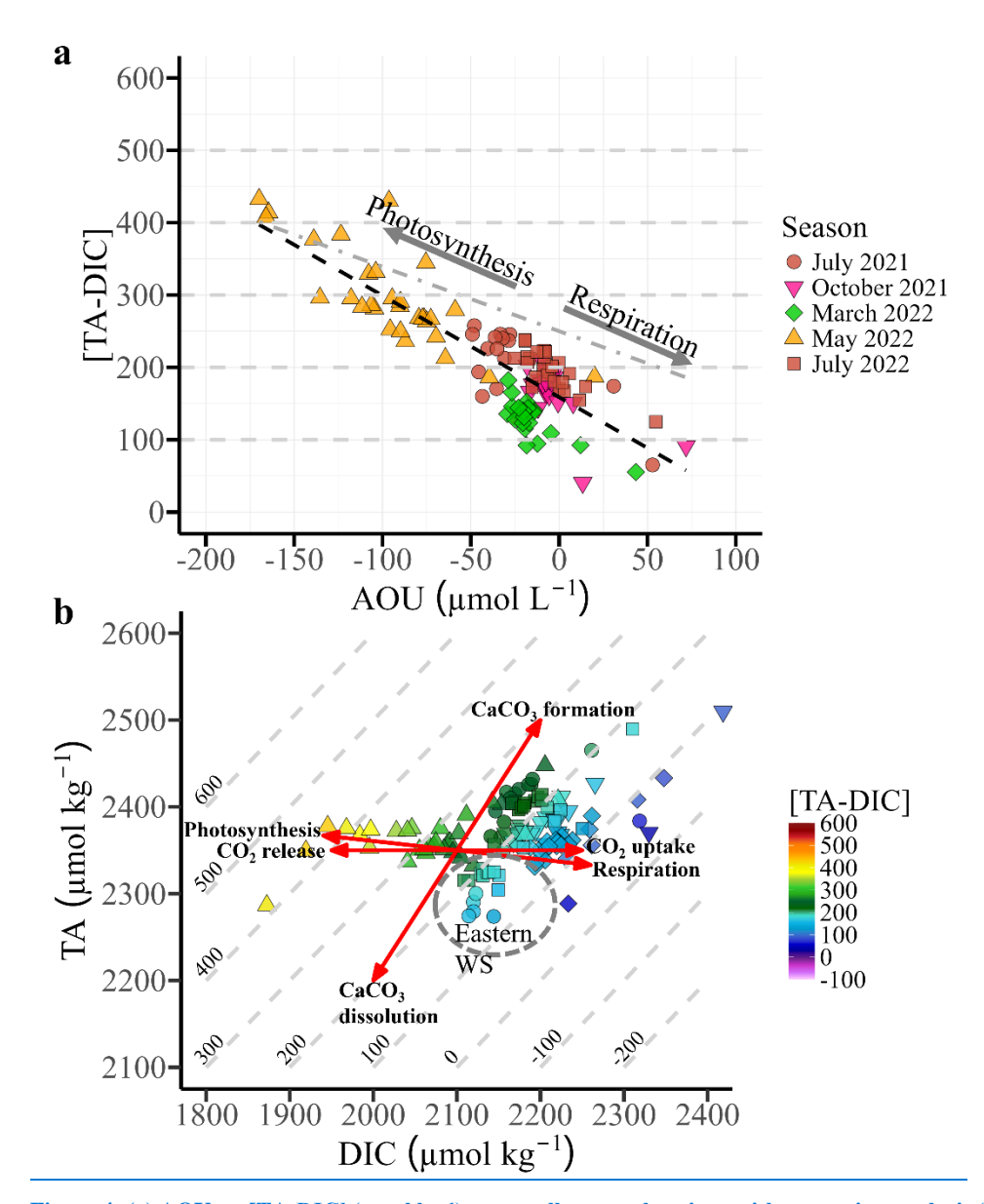


Figure 4: (a) AOU vs. [TA-DIC] (μmol kg⁻¹) across all seasonal cruises, with regression analysis (black dashed line). Arrows indicate potential processes affecting [TA-DIC] and apparent oxygen utilization (AOU). The grey dashed line represents the regression slope (-123 / 138 = -0.89) proposed by Xue and Cai (2020). (b) DIC versus TA plot from all seasons, with the coloured values of [TA-DIC] for the EFWS at salinity 25 – 32.5. Isoclines represent [TA-DIC] values. Red lines indicate key biogeochemical processes (photosynthesis / respiration, CO₂ exchange, and CaCO₃ formation / dissolution). The Eastern EFWS is highlighted with a grey circle.

3.4 Seasonal Variability of DIC and TA in the EFWS: Influence of Mixing Processes

425

Stations located near Norddeich harbour, closer to the mainland, exhibit extreme values (Fig. 2) and therefore were excluded from the calculation of mean \pm standard deviation to provide a more representative assessment of ΔDIC_{excess} , ΔTA_{excess} , and

 ΔTA_P . However, these values are still displayed in the scatter plots (Fig. 5) to illustrate the range of variability, including highly positive and negative deviations.

The Western WS generally exhibits positive ΔDIC_{excess} values, with a peak in October 2021 (47.7 ± 84.9 μmol kg⁻¹) and July 2022 (54.6 ± 33.3 μmol kg⁻¹), suggesting an excess of DIC beyond the expected mixing (Fig. 5a). In contrast, during May, ΔDIC_{excess} in the Western WS was negative (-69.3 ± 107.0 μmol kg⁻¹), suggesting significant DIC consumption, potentially due to enhanced primary production during spring bloom conditions. Similarly, negative values were observed in the Eastern WS in May 2022 (-30.1 ± 35.8 μmol kg⁻¹) and July 2021 (-19.3 ± 11.2 μmol kg⁻¹) (Table 4; Fig. 5a).

435

440

Higher $\Delta TA_{\text{excess}}$ values are observed in the Western WS, particularly in July 2021 (123.0 ± 27.8 µmol kg⁻¹), indicating additional alkalinity sources. In spring, $\Delta TA_{\text{excess}}$ showed a clear positive trend, with an increase from March to May in both regions (Fig. 5b), suggesting that while TA is being consumed, production still exceeds consumption. The increases in TA from March to May were $20.0 \pm 42.22 \ \mu\text{mol kg}^{-1}$ in the Western WS and $8.1 \pm 18.62 \ \mu\text{mol kg}^{-1}$ in the Eastern WS (Table 4; Fig. 5). The Eastern WS exhibits lower $\Delta TA_{\text{excess}}$ values, with some negative values in July 2022 (-34.7 ± 32.3 µmol kg⁻¹), when the sluice was open. ΔTA_{P} , representing primary production effects, is positive in May (Table 4; Fig. 5c) in the Western and Eastern WS, indicating a net uptake of CO₂ through biological processes and a corresponding decrease in DIC (Fig. 5a).

Table 4: Overview Mean \pm Standard Deviation of different the parameters TA (μ mol kg⁻¹), DIC (μ mol kg⁻¹) Δ DIC_{excess}, Δ TA_{excess}, and [TA-DIC] Δ TA_P (μ mol kg⁻¹) of all seasonal samplings easons in average with the standard deviation the Eastern and Western EFWS.

Parameter Seas	July 2021	October 2021	March 2022	May 2022	July 2022
on	-			-	
TA (µmol kg ⁻¹)					
ADIC excess	$\frac{2403}{23}$.4 ± 27.46	$\frac{2406}{47}.7 \pm \frac{53.8}{8}$	$2358.6 \pm 2720.5 \pm 2$	2378.9 ± 39.0	238054.6 ± 33.3
Western WS:	$\frac{2283.5 \pm 10}{2}$	<u>4.9</u>	<u>3</u> .8	2349.7 ± 9.8	$-16.0 \pm 26.2 \pm 42.7$
Eastern WS:	19.3 ± 11.2	<u>-</u> 6	$\frac{2347.25.85}{11.8}$	2741-69.3 ± 77.4 107.0	2337.2 ± 35.2
Ems Estuary:	_	$\frac{2367.8 \pm 5.3}{}$	$\frac{2609.2 \pm 68.0}{}$	-30.1 ± 35.8	$\frac{2697.7 \pm 101.1}{}$
		37 ± 19.4			
DIC (μmol kg ⁻¹)					
<u>ATA</u> excess	$2185123.0 \pm 27.8 \pm 4$	2257.1 ± 91.0	$\frac{2237}{16.6 \pm 21.9}$	2065.5 ± 107.0	$2184.4 \pm 4350.9 \pm 2$
Western WS:	8.2	2182.8 ± 18.2	10.7 ± 37.8	2089.2 ± 38.0	<u>1.9</u>
Eastern WS:	$\frac{2124.1 \pm 10.3}{}$	-29.9 ± 51.9	2211.8 ± 11.8	$2791.5 \pm 136.036.6 \pm 3$	-34.7 ± 32.3
Ems Estuary:	-9 ± 11.5	-2.35 ± 5.87	$2681.3 \pm 124.412.5$	6.1	2142.3 ± 27.6
				18.8 ± 13.8	2682.6 ± 169.1
[TA DIC]					
(µmol-kg⁻¹)					
$\Delta T A_P$	217.55 ± 51.9	$150.5 \pm 47{-}$	$\frac{120.9 \pm 30.2}{}$	313.3 ± 7611.1	196. -
Western WS:	159.44 ± 16.4	7.65 ± 13.6	137.9 ± 11. -	$\frac{260.5 \pm 34.7}{}$	$8 \pm 26.7.75 \pm 5.35$
Eastern WS:	-3.75 ± 4.43	1	3.28 ± 3.82	$-50 \pm 17.2 \pm 77.6$	$\frac{194.9 \pm 21.1}{}$
Ems Estuary:	3.10 ± 1.80	184.9 ± 19.9	<u>-</u> 0	4.83 ± 5.74	$15.1 \pm 69.2.56 \pm 4.2$
-		02 ± 3.11	-		<u>0</u>
			<u>.845 ± 1.</u> 72 .1 ± 70.7		

The mean measured TA in the Western WS in May 2022 was 2378.9 μmol kg⁻¹ in the intertidal zone (Table 3, Fig. 7), indicating a slight increase in TA from March to May 2022. Most of the TA in the intertidal zone are close to or above the mixing line, with similar negative slopes in the Western WS (15.6 μmol kg⁻¹ per salinity unit) and in the Eastern WS (15.3 μmol kg⁻¹).

μmol kg⁻¹ per salinity unit) (Fig. 8g). The lowest DIC values (down to 1872 μmol kg⁻¹) in this study were also measured in the intertidal zone of the Western WS in spring (Table 3; Fig. 7; Fig. 8h). The DIC concentration in May 2022 was the lowest overall measured in this study, which is why the DIC values are below the mixing line (Fig. 8h).
 During all seasons, the TA concentration was higher than the measured DIC concentration, which can be seen in the positive values of [TA DIC] (Table 3). The highest positive [TA DIC] was calculated in May 2022, followed by the summer seasons (July 2021, July 2022), October 2021 and March 2022. The lowest [TA DIC] was calculated in March 2022 and October 2021 (Table 3). The three lowest [TA DIC] values in October 2021, March 2022 and July 2021 were the stations, which are located next to the harbour Norddeich. As described above, these showed already differences to the other stations in the parameters of the FerryBox (Fig. 3; Fig. 4).

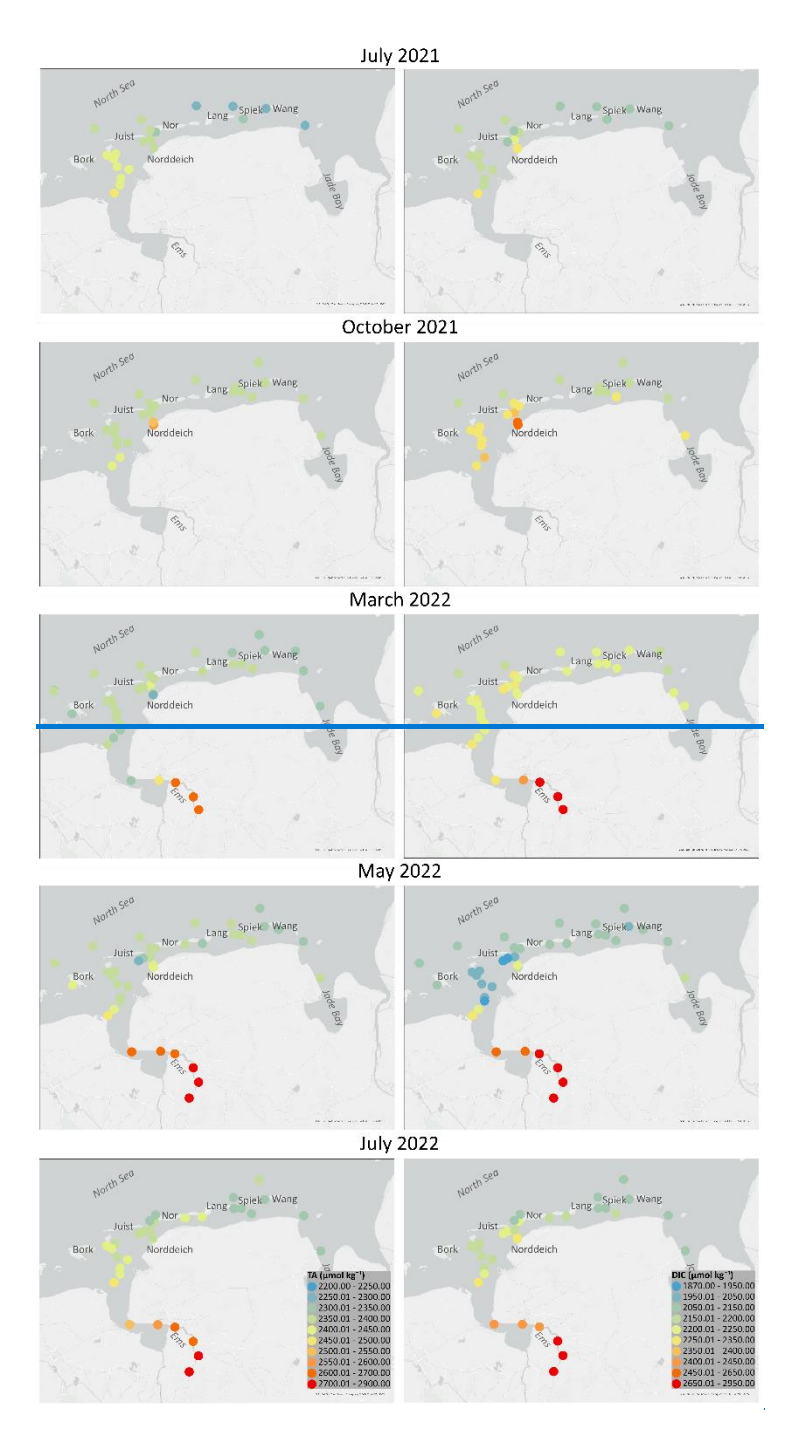


Figure 7: Measured results of TA and DIC of all seasonal cruises of July 2021, October 2021, March 2022, May 2022 and July 2022. All TA and DIC values are in µmol kg 1). The map in this Figure was generated using AreGIS. Data sources: LGLN, Esri, TomTom, Garmin, Foursquare, FAO, METI/NASA, USGS. © 2024 Julia Meyer.

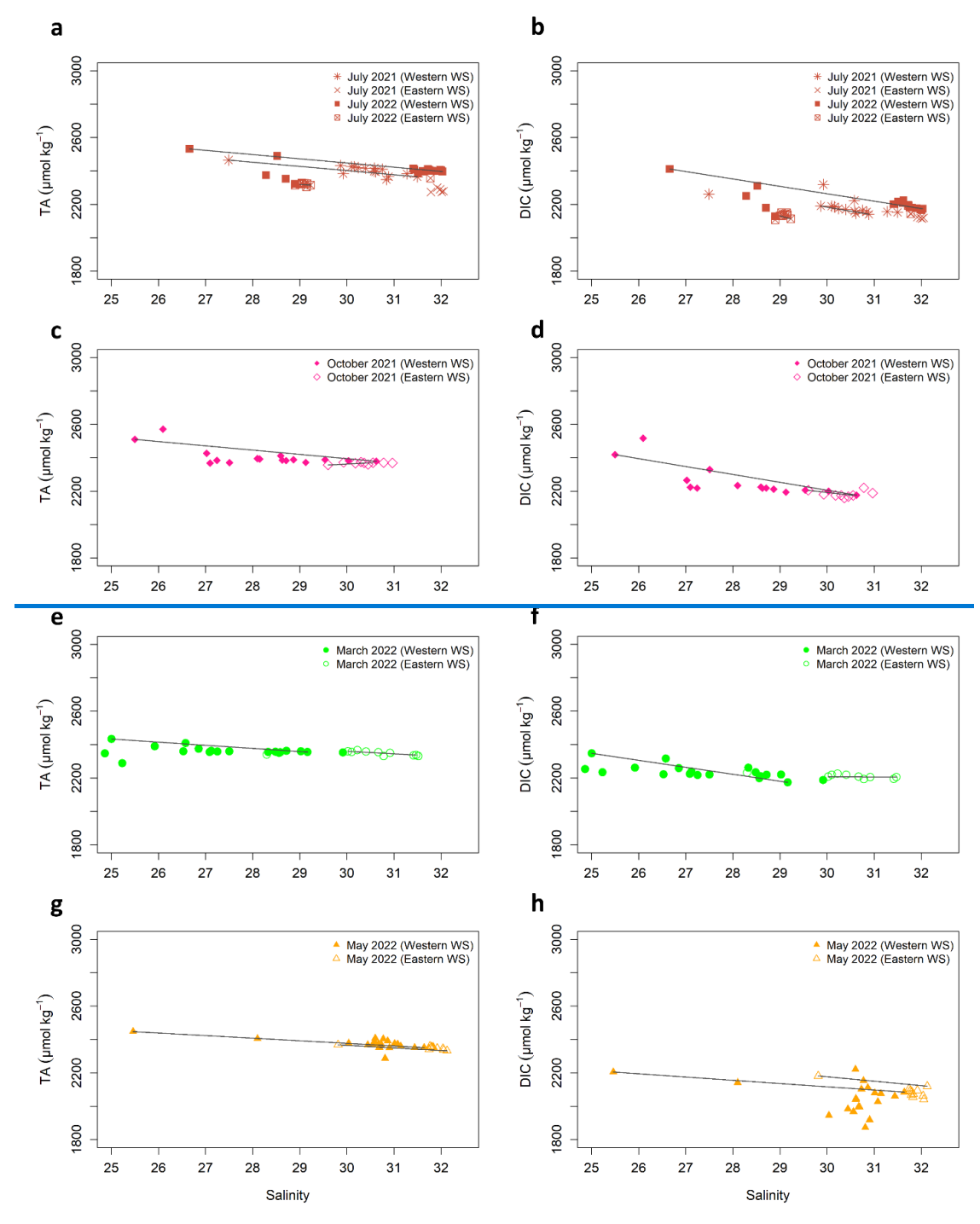


Figure 8: TA (μ mol kg⁻¹) and DIC (μ mol kg⁻¹) mixing plots, against salinity of July 2021 (a, b), October 2021 (c, d), March 2022 (e, f), May 2022 and July 2022 (a, b) at > 25 salinity, separated by the different regions (Eastern WS, Western WS) of the studied intertidal East Frisian WS.

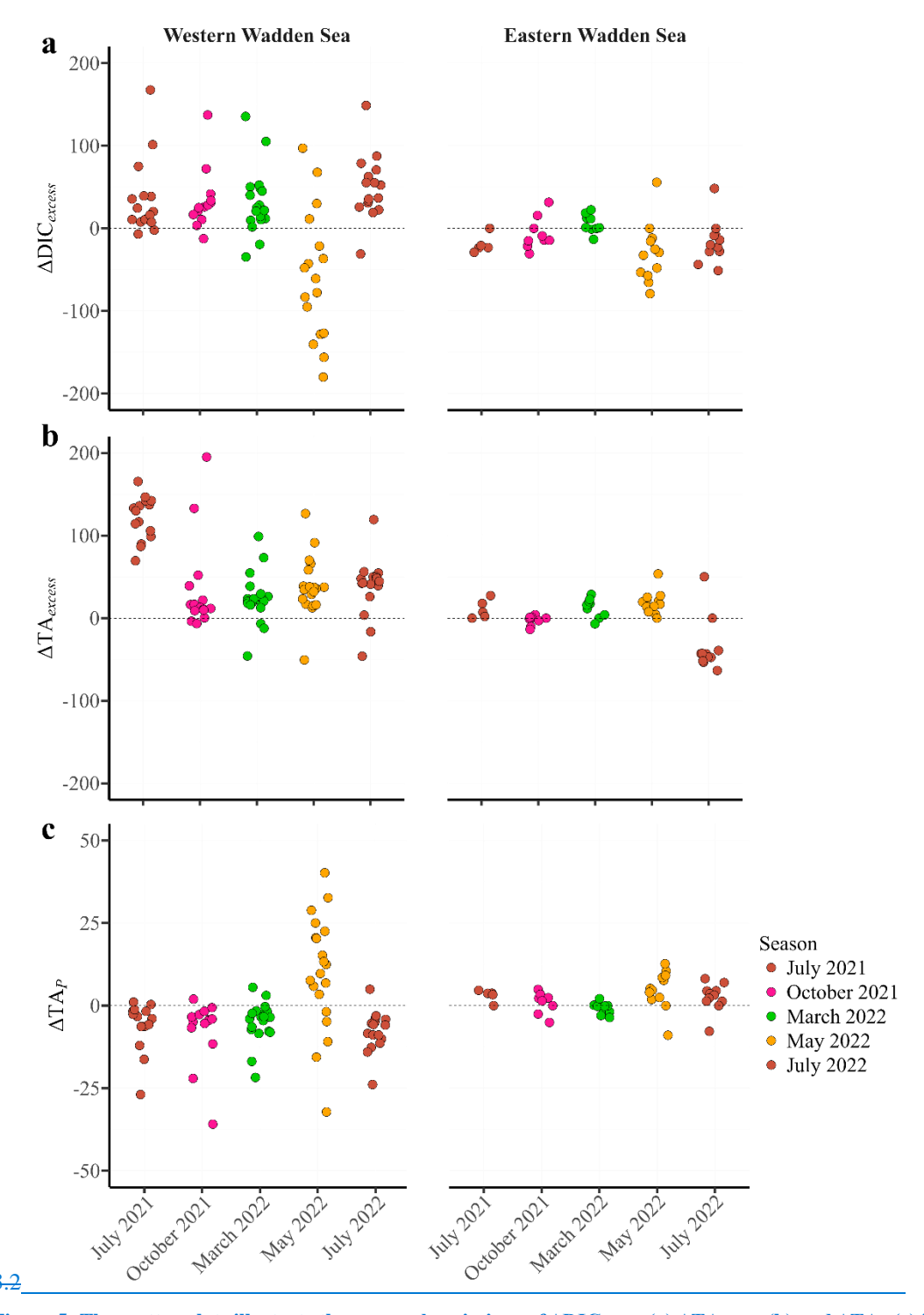
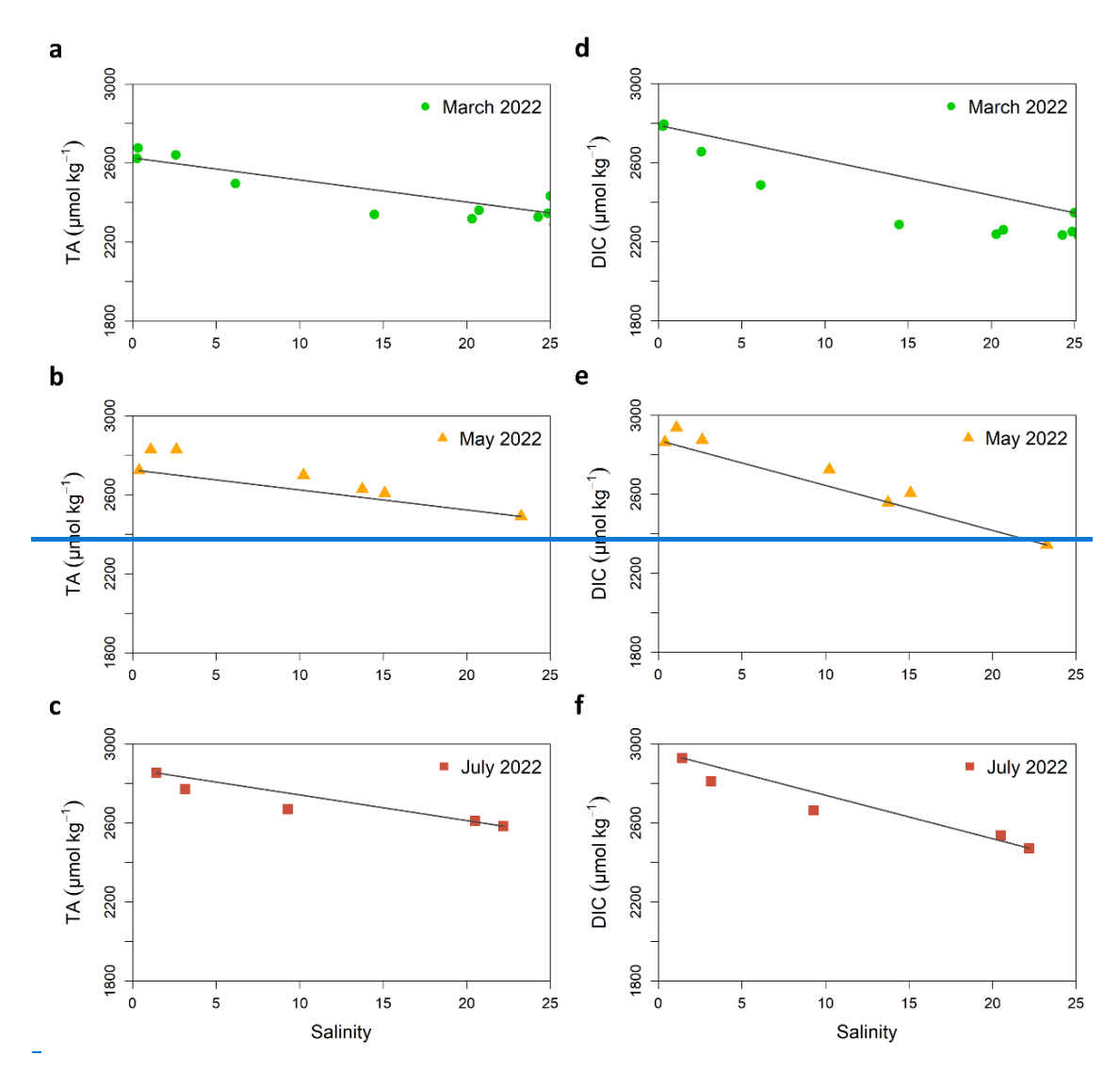


Figure 5: The scatter plots illustrate the seasonal variations of ΔDIC_{excess} , (a) ΔTA_{excess} , (b) and ΔTA_{P} (c) in μ mol kg⁻¹ in the Western WS (left panels) and Eastern WS (right panels) from each season. Each colour represents different seasons.

3.5 Regional and seasonal variation of the Ems River Estuary Nutrients



470 Figure 9: TA (μmol kg⁻¹) and DIC (μmol kg⁻¹) mixing plots, against salinity of July 2021 (a, b), October 2021 (c, d), March 2022 (e, f), May 2022 and July 2022 (a, b) at > 25 salinity, separated by the different regions (Eastern WS, Western WS) of the studied intertidal East Frisian WS.

Within the Ems River Estuary the temperature was lowest in March 2022 (down to ~5 °C) and highest (up to 21.9 °C) in July 2022 (Table 2; Fig. 2). The turbidity in the Ems River estuary increased with lower salinity during all seasons, with decreasing pH (down to 7.33) (Fig. 2). The chlorophyll a was relatively low to the intertidal WS in March 2022 (down to ~9 μg L⁻¹) and in July 2022 (down to 11.9 μg L⁻¹) (Table 2; Fig. 3). Chlorophyll a was higher in May 2022 (up to 25.1 μg L⁻¹) than in other periods in the Ems River estuary at the lowest salinity level (17.60) where chlorophyll a was measured (Table 2; Fig. 3). Overall, the oxygen saturation was also lower in the Ems River estuary compared to the intertidal WS, down to 62.8 %sat in

March 2022 (Fig. 3). Oxygen saturation decreased further with decreasing salinity in May 2022 and July 2022 to 20.2 %sat and 13.44 %sat respectively (Fig. 3). The $pCO_{2 \text{ obs}}$ concentration showed the vice vera picture of oxygen saturation, which increased with decreasing salinity (Fig. 4). The $pCO_{2 \text{ obs}}$ was observed from March 2022 to May 2022 in the Ems River estuary, with values reaching 2307 \pm 534 μ atm in March and 1522 \pm 1318 μ atm in May. The calculated difference between these values is 785 \pm 1421 μ atm, indicating significant variability (Fig. 4).

The Ωcal dropped with decreasing salinity in the Ems River estuary and remained undersaturated (> ~ 0.8) during all seasons, leading to shells and skeletons made of CaCO₃ to become vulnerable to dissolution (Table 2; Fig. 5). In the Ems River estuary, the measured TA and DIC increased with lower salinity during all seasons (Fig. 7; Fig. 9). Maximum TA values of 2676 μmol kg⁻¹ were recorded in the Ems River estuary in March 2022, while values in the intertidal zone were lower (Table 2; Fig. 7; Fig. 9). However, [TA DIC] cannot be used at low salinity (e.g. <20) and when [TA DIC] is < ~50 μmol kg⁻¹, where the relationships of [TA DIC] with pH and/or ocean acidification are nonlinear, these low values also occur in oxygen minimum zones (Xue and Cai 2020). This is the reason, why we only are showing the results of the intertidal region of the East Frisian WS (Western WS, Eastern WS) (Table 3, Fig. 14, Fig. 15).

The Ems River estuary shows highest NO₃⁻ concentrations in March 2022 (up to 341.47 μ mol L⁻¹), decreasing also in summer (down to 97.50 μ mol L⁻¹) (Fig. 12), yet remains also high. In contrast, NH₄⁺ was also high in in the Ems River estuary in March 2022, however it dropped constantly from 19.73 μ mol L⁻¹-down to the detection limits > 0.01 μ mol L⁻¹. NO₂⁻ concentrations also dropped from March 2022 to May 2022 (Fig. 12).

3.3 Regional Variability and Seasonal Trends in ADICexcess and ATAexcess in the Wadden Sea

480

485

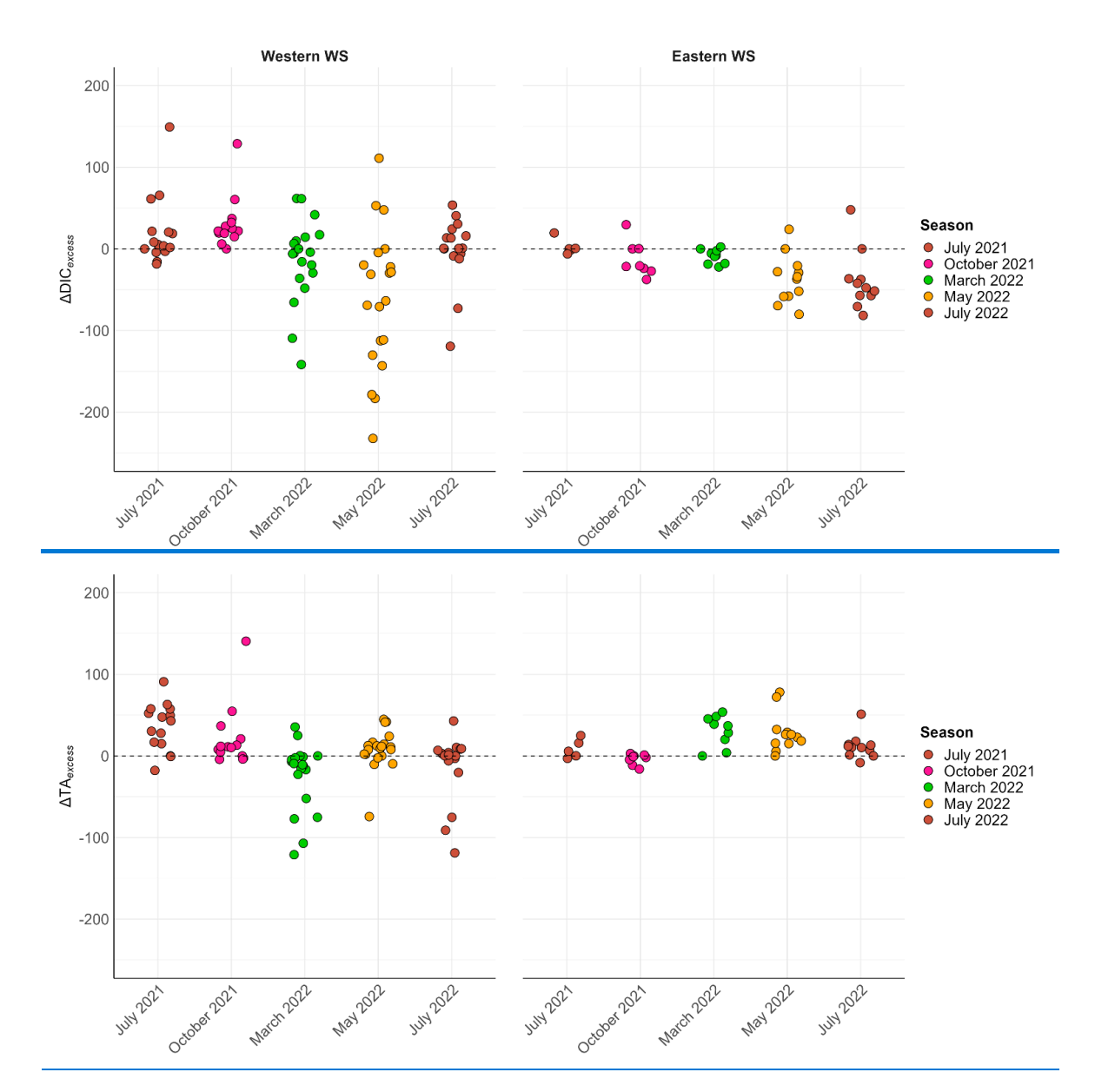
490

495

500

505

Higher fluctuations in the Western WS in comparison to the Eastern WS were observed in ΔDIC_{excess} and ΔTA_{excess} (Fig. 10), seasonally and regionally. In the Western WS ΔDIC_{excess} values were mostly positive in July 2021, October 2021 and in July 2022, indicating production of DIC (Fig. 10). This was also observed in other parameters described before and in the mixing plots of TA and DIC with salinity (Fig. 8). The mean ΔDIC_{excess} for the Western WS in March 2022 ($14.2 \pm 51.5 \,\mu$ mol kg⁻¹) shows more stations consuming than producing DIC (Fig. 10). This pattern of DIC, with stations above and below the mixing line, is also shown in Fig. 7f. The greatest variability of ΔDIC_{excess} is observed in May 2022 ($60.9 \pm 84.4 \,\mu$ mol kg⁻¹) in the Western WS with some outlying values next to the Norddeich harbor above zero (Fig. 8; Fig. 10). If we treat the two stations near the port of Norddeich as outliers in July 2022, which are strongly negative in Fig. 10, we obtain positive mean values for ΔDIC_{excess} (11.9 \pm 18.7 μ mol kg⁻¹) in the WS, which means that production exceeds consumption of DIC. This was not very clear in the mixing plot shown in Fig. 8b, however.



10 Figure 10: Calculated ΔDIC_{excess} and ΔTA_{excess} values of all seasons in on the Eastern WS and Western WS in μmol kg⁻¹of each season.

Excluding the strongly negative values of $\Delta TA_{\text{excess}}$ (Fig. 10) and treating them as outliers in July 2022 in the Western WS, we obtain a positive mean of 4.5 ± 13.5 , indicating production, as evident in Fig. 8a. In contrast, higher mean value of $\Delta TA_{\text{excess}}$ (35.6 \pm 27.9 μ mol kg⁻¹) in July 2021 implies a higher production in TA (Fig. 8a; Fig. 10) in the Western WS. The $\Delta TA_{\text{excess}}$ values in October 2021 are mostly close to zero, except for the stations close to land (Norddeich). If we exclude these stations, the mean $\Delta TA_{\text{excess}}$ value of $12.4 \pm 16.3 \mu$ mol kg⁻¹, indicating slight production of TA (Fig. 10). This finding, however, is

western WS may be contributing to the observed changes in TA (Fig. 8c). In March 2022, negative ΔTA_{excess} values were measured near the Ems River estuary, suggesting consumption of TA in this region. However, positive values (ranging from ~10 – 50 μmol kg⁻¹) in the intertidal region around Juist and Norderney indicate production of TA. Despite these observations, the mixing plot does not show a clear pattern of TA production and consumption (Fig. 8e), indicating a mixing effect of riverine water masses coming from the Ems River estuary (Fig. 10). In May 2022, the ΔTA_{excess} values suggest a slight production of TA. Almost all values, except for one strongly negative station located near Juist, are positive, resulting in a mean value of 8.2 ± 8.7 μmol kg⁻¹ (Fig. 10). This slight positive trend is also visible in Fig. 8g, where most points are positioned just above or on the mixing line.

520

525

530

535

540

545

The Eastern WS exhibits lower variability in ADIC and ATA access. In October 2021 and March 2022, ADIC access values were close to zero, with mean values of 2.5 ± 10.4 µmol kg⁻¹ and 9. ± 8.3 µmol kg⁻¹, respectively (Fig. 10). This pattern suggests a slight production of DIC in October 2021 and consumption in March 2022 (Fig. 8f), however, this was not clearly evident in the mixing plots shown in Fig. 8, which may be due to higher riverine influence. In May 2022, predominantly negative ΔDIC_{excess} values were observed, with a mean value of $36.9 \pm 28.2 \ \mu mol \ kg^{-1}$ (Fig. 10). This pattern is likely attributable to photosynthesis, which is especially pronounced in spring. The lowest variability in ADIC. was observed in July 2021 with a mean value of 8.7 ± 10.6 µmol kg⁻¹, suggesting slight production of DIC, lower to the Western WS (Fig. 10). The ΔTA_{excess} shows a similar pattern in July 2021 (mean value of $8.7 \pm 10.4 \, \mu \text{mol kg}^{-1}$) and July 2022 (mean value of 11.7 ± 14.4 µmol kg⁻¹), both indicating a production of TA (Fig. 8; Fig. 10). Nevertheless, only a small number of stations were available for this calculation within the season, and only the Weser River was included in the Eastern WS, highlighting the importance of also considering other rivers like the Rhine and the Elbe. Additionally, the time periods of river sampling for the calculation of ΔDIC_{excess} and ΔTA_{excess} values did not always coincide exactly with the sampling times during the RV Burchana cruises. Such discrepancies could lead to deviations, meaning that the results can only indicate a general trend or seasonal pattern. This is also evident in the results from July 2022, where the ΔDIC_{excess} displays a different pattern compared to the Western WS. While a negative mean value of 39.5 ± 34.1 µmol kg⁻¹ ADIC_{excess} was calculated in the Eastern WS. positive ADIC_{excess} values (11.9 ± 18.7 µmol kg⁻¹) was determined in the Western WS (Fig. 10). It is important to note that on July 11, the Eastern WS was influenced by the opening of the sluice at Neuharlingersiel, which altered salinity during the sampling day and lower TA and DIC concentrations (Fig. 7; Fig. 8a, b; Fig. 10). As a result, the consumption of DIC and production of TA in the Eastern WS could partly be attributable to land based inputs (Fig. 2; Fig. 8a, b; Fig. 10), decreasing the real signal of TA production and DIC consumption in this region.

3.4 Estimation of TA generation via primary production and nutrient dynamics

For ΔTA_P, greater variability is visible in the Western WS compared to the Eastern WS regionally (Fig. 11). At different times, there are both positive and negative deviations from the zero line, indicating periodic fluctuations in photosynthetic activity with TA production and TA consumption due to other processes (e.g., respiration, CaCO₃ precipitation). While the values of

ATA_P exhibit lower variability in July 2021 and October 2021, except for the stations near the Norddeich harbor, the other seasons show greater variability. Thus, a mean value of 3.4 ± 6.6 μmol kg⁻¹ in July 2021 and a mean value of 5.1 ± 13.3 μmol kg⁻¹ in October 2021 (excluding the stations near Norddeich) can be observed (Fig. 11). This indicates a lower effect from photosynthesis, suggesting that other biogeochemical processes contribute to TA production during these seasons (Fig. 11).

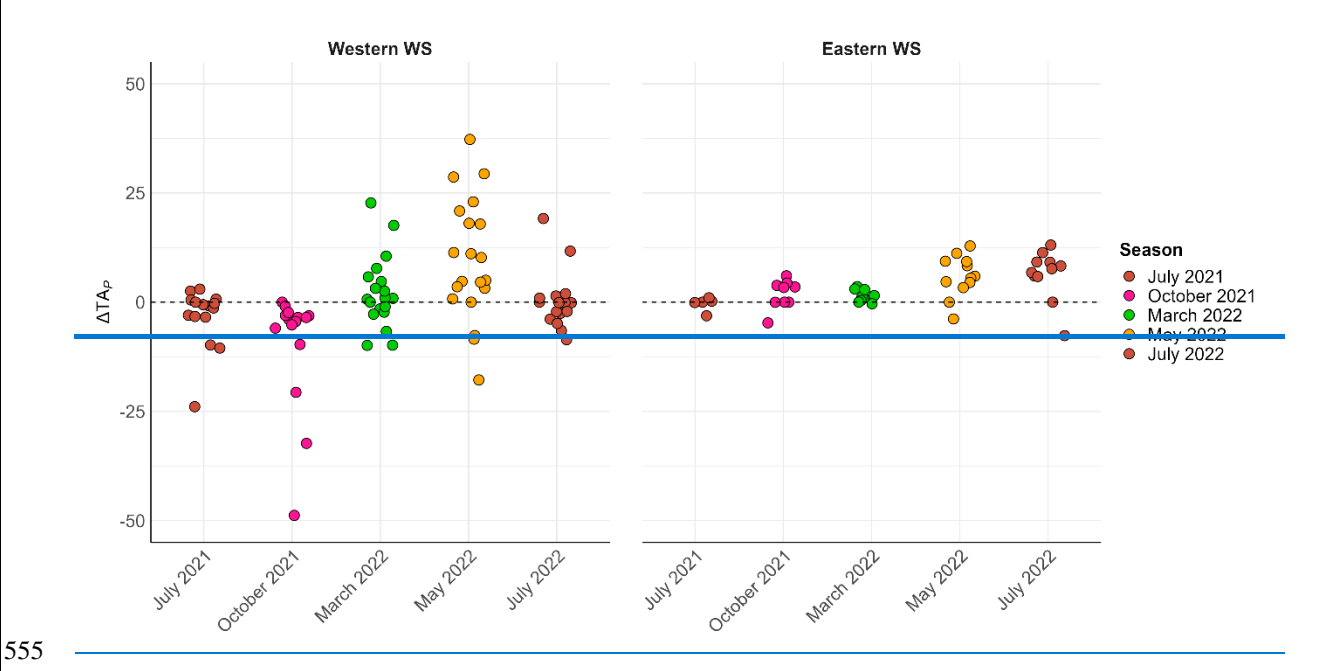


Figure 11: Calculated ATAP values in µmol kg-1 of all seasons in the Western WS and Eastern WS.

550

560

565

In the Western WS, the mean value was $2.3 \pm 8.0 \,\mu\text{mol kg}^{-1}$ in March 2022 and $9.8 \pm 6.6 \,\mu\text{mol kg}^{-1}$ in May 2022. Therefore, March 2022 and May 2022 show a wide range of ΔTA_P values, with many data points above zero, indicating as higher tendency to biological productivity due to primary production, generating TA (Fig. 11) driven by decreasing NO_3^- concentrations from March to May 2022 (Fig. 12). Overall, approximately 80% of the sampled stations had positive ΔTA_P values ($\Delta TA_P > 0$) in May, indicating TA production can be explained by primary production (Fig. 10). In July 2022, the ΔTA_P values were more dispersed, with a mean value of $0.3 \pm 6.5 \,\mu\text{mol kg}^{-1}$. Around 40% of the stations had positive values, while approximately 60% of the values were negative in July 2022. This suggests that primary production and other biogeochemical processes contribute to the generation of TA in the Western WS (Fig. 10; Fig. 11).

The ΔTA_P values in the Eastern WS exhibit less variability compared to the Western WS. Most data points are clustered around zero across all seasons, indicating minimal changes in alkalinity. There are fewer stations and extreme values in the Eastern WS, suggesting more stable alkalinity production over the observed seasons. The highest variability of ΔTA_P in the Eastern WS was measured in May (5.9 \pm 4.5 μ mol kg⁻¹) and July 2022 (6.3 \pm 5.5 μ mol kg⁻¹). TA production is also visible here in May 2022, but not as pronounced as in the Western WS, where we encountered signals of higher biological productivity (Fig. 11).

Once again, it is important to mention that the opening of the Neuharlingersiel sluice may possibly have influenced the values of ATA_P in July 2022 (Fig. 11).

A clear seasonal pattern can also be seen in the measured nutrients (Fig. 12S4). For NO₂⁻ and NH₄⁺ a decrease in concentrations was observed from October 2021 to May 2022, except in the East part of the East Frisian WS for NO₂-EFWS (Fig. 12S4), where the concentration did not change much. NO₃⁻ concentration ranged seasonally, with an increasing trend from summer to March 2022 (up to 66.28 μmol L⁻¹) in the intertidal East Frisian WS.EFWS. In May 2022, the NO₃⁻ concentrations decreased again below the detection limit of the instrument (> 0.01 μmol L⁻¹) at some stations, mainly in the Western part (Fig. 12S4). This analogous seasonal tendency possibly will point to common sources and sinks.

575

580

585

Overall, from March 2022 to May 2022 there was an average decrease in NO₃⁻ of 19.29 ± 18.11 µmol kg⁻¹ (Fig. 13; Fig. 136). TA slightly increased by $9.1 \pm 29.2 \,\mu$ mol kg⁻¹ during this time (Fig. 7 Fig. 8; Fig. 10; Fig. 114 - 6), while DIC decreased on average by $159.4 \pm 125.4 \,\mu$ mol kg⁻¹ (Fig. 7; Fig. 8; Fig. 10). The differences of NO₃⁻ and SiO₂ for all stations between March and May 2022 (Δ NO₃⁻, Δ SiO₂) were plotted against the DIC difference between March and May (Δ DIC, Fig. 136). For Δ NO₃⁻ a regression line was fitted with equation of $y = 6.90x + 29.089 \,(R^2 = 0.4637, p$ - value = < 0.05, Fig. 136), while the Δ SiO₂ regression has an equation of $y = 8.11x + 50.605 \,(R^2 = 0.2165, p$ - value = < 0.05, Fig. 136). The slope of both regression lines is close to the Redfield Ratio (Redfield et al., 1963) of $106/16 = 6.625 \,\text{for NO}_3$ ⁻ (6.90, Fig. 136) and $106/15 = 7.067 \,\text{for SiO}_2$ (8.11, Fig. 136), indicating that the identified enhanced primary production in this region in the spring, along with nutrient (nitrate) uptake of the available inorganic nutrient species most likely lead to a concomitant decrease in DIC (Fig. 13).6) and increase TA.

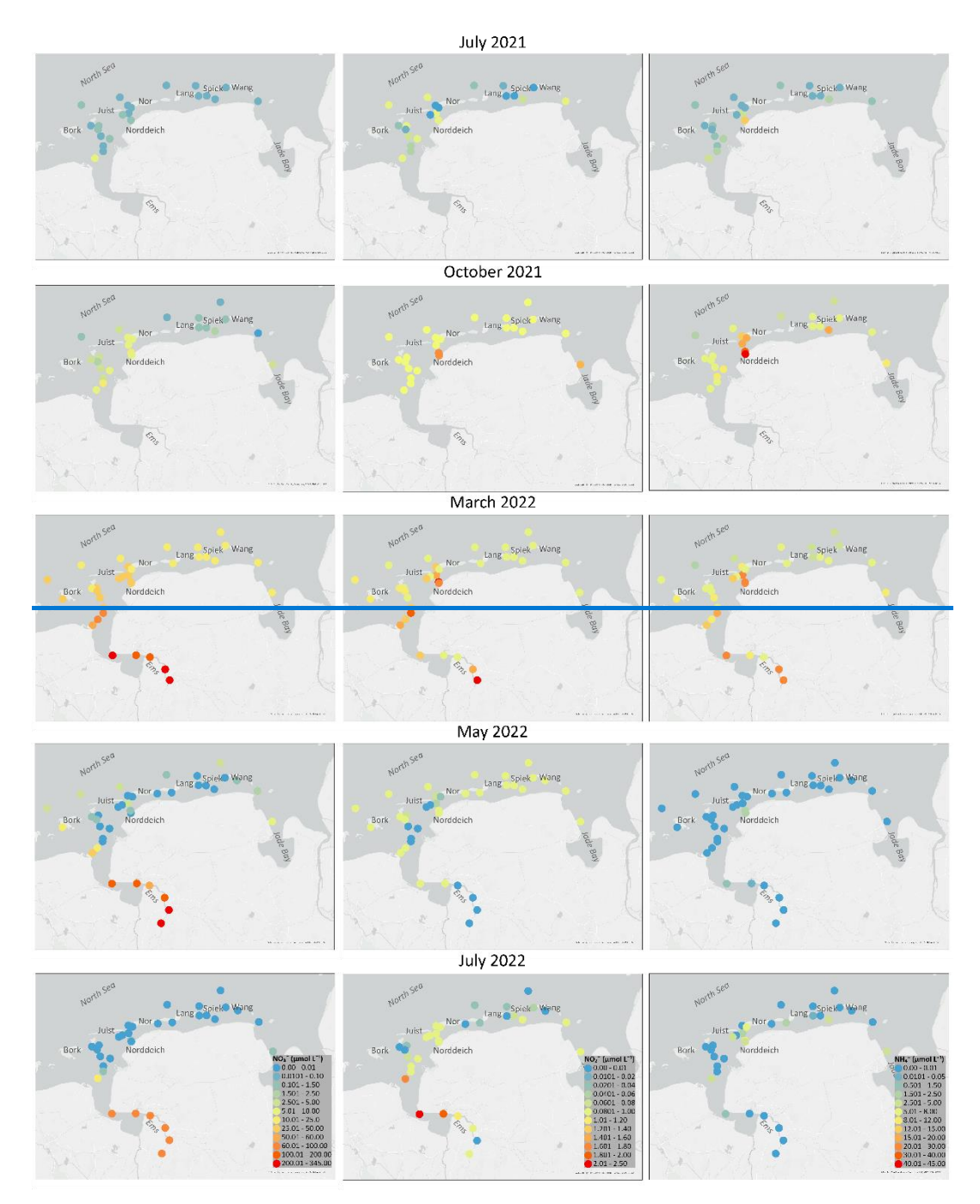
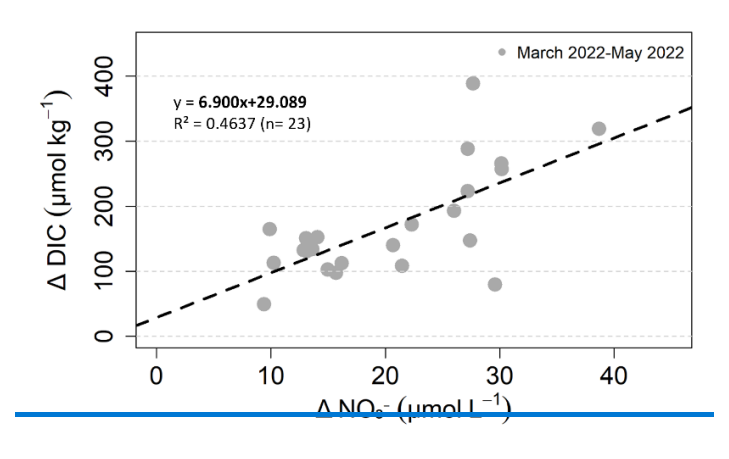


Figure 12: Measured nitrate (NO₃- in μmol L₋₁), nitrite (NO₂- in μmol L₋₁) and ammonium (NH₄₊ in μmol L₋₁) of all seasonal cruises from July 2021 until July 2022. The map in this Figure was generated using ArcGIS. Data sources: LGLN, Esri, TomTom, Garmin, Foursquare, FAO, METI/NASA, USGS. © 2024 Julia Meyer.



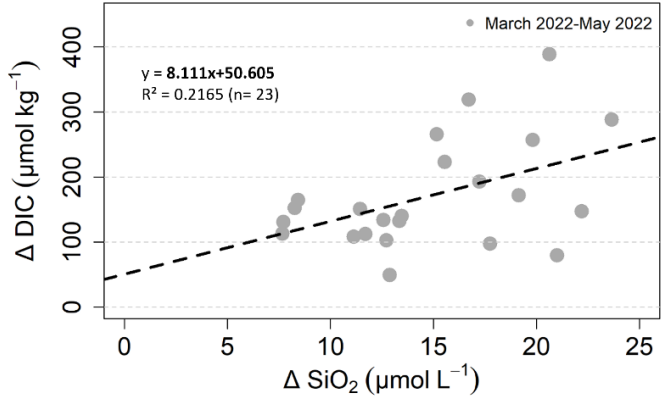


Figure 13

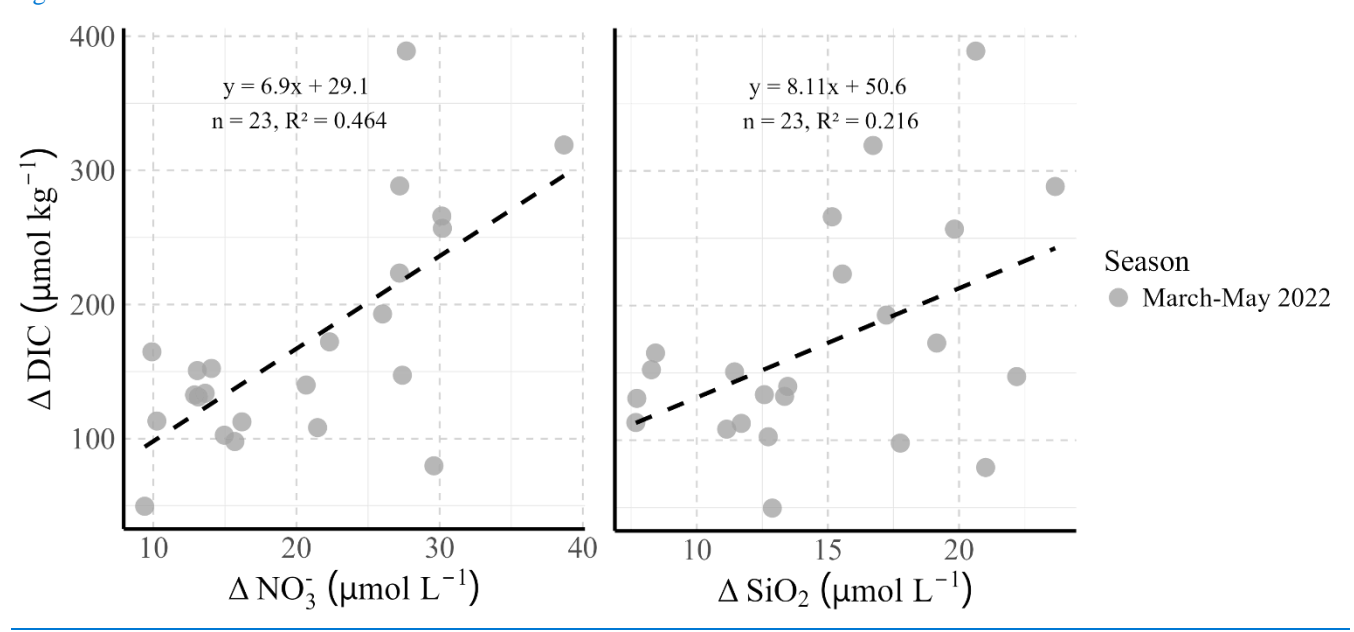


Figure 6: NO₃ and SiO₂ differences (ΔNO₃, ΔSiO₂) of March to May 2022 against the difference of DIC (ΔDIC), with the related regression equations. The slopes show the Redfield Ratios of all measured stations in the Western and Eastern WS.

4-Discussion

600

605

4.1 Regional and seasonal Differences of the Carbonate Dynamics in the Carbonate System of the East Frisian Wadden Sea-EFWS

Coastal oceans and shelf seas, such as the North Sea, exhibit significant variability (Blackford and Gilbert, 2007), a phenomenon also observed in the carbonate system of the East Frisian WS. The This study highlights regional and seasonal variability in the carbonate system of the East Frisian WS. Notably, there is a pronounced, with a notable West-to-East gradient in DIC and TA, with both showing considerable fluctuations across seasons.

Seasonal biological production appears to enhance TA, especially in spring and summer, potentially increasing the region's capacity for carbon dioxide uptake. However, the TA variability in the coastal ocean is more complex, due to other processes like evaporation, coastal shelf circulation and tidal dynamics, upwelling, sulfate reduction, denitrification, nitrification and calcium carbonate calcification and dissolution (Abril et al., 2003; Böttcher et al., 1998; Brewer and Goldman, 1976; Cai et al., 2010; Cao et al., 2011; Chen and Wang, 1999; Faber et al., 2014; Hoppema, 1990; Liu et al., 2012; Onken and Riethmüller, 2010; Postma, 1981; Voynova et al., 2019; Wolf Gladrow et al., 2007).

4.2 [TA-DIC] as a proxy for Biogeochemical Processes Driving Carbonate Dynamics

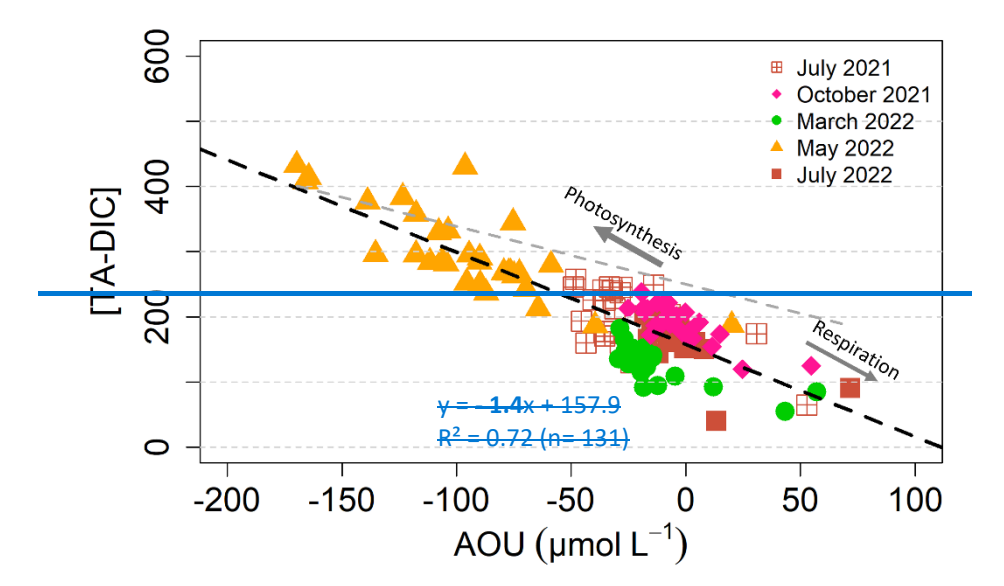
610

615

625

630

Previous studies have shown that [TA DIC] can be used to identify the influence in (Table 3; Fig. 2). This is the first study to investigate ΔDIC_{excess}, ΔTA_{excess}, ΔTA_e



620 Figure 14: AOU relationship to [TA-DIC] in μmol kg 1 of all seasonal cruises with the related regression analysis (black dashed line). The arrows show the possible processes that could affect the [TA-DIC] and apparent oxygen utilization (ΛΟU). The grey dashed 475 line represents the regression line, which illustrates the Redfield ratio slope (-123/138 = -0.89), proposed by (Xue and Cai, 2020).

Figure 14 presents data from all stations in the WS sampled during different seasons and the calculated AOU relationship to [TA DIC], which we can directly link to the Redfield ratio (Redfield, 1963). This information is essential to understand the role of the biological carbon pump and the influence on biogeochemical processes (Xue and Cai, 2020). However, it is important to note that these samples were collected exclusively during daylight hours, excluding the night cycle. This likely skews the data towards conditions that favor photosynthesis over respiration, as photosynthesis occurs during the daylight hours, while respiration continues both day and night. We therefore measured predominantly negative AOU values and an increase in [TA DIC] due to reduced DIC (Fig. 14). The microphytobenthos in the Northern German WS for example was found to significantly impact the local carbon cycle through photosynthesis, producing oxygen and consuming CO₂ during the day (Wolfstein et al., 2000). This aligns with the observed negative AOU values and higher [TA DIC], as photosynthesis

would rise [TA-DIC] by consuming CO₂ and generating oxygen, thus affecting AOU (Fig. 14). In contrast, respiration, which occurs continuously both day and night, increases AOU, leading to positive values, and decreases [TA-DIC], as more dissolved inorganic carbon is produced through the decomposition of organic material. Specifically, the respiration of 1 mole of organic matter ((CH₂O)₁₀₆(NH₃)₁₆H₃PO₄) increases DIC by 106 moles and decreases TA by 17 moles (Chen 1978). This results in a change of 123 moles in [TA-DIC] (Xue and Cai, 2020).

635

640

645

650

655

660

665

The regression of Fig. 14 shows a negative correlation between ITA DICI and AOU with a negative slope of 1.416 umol kg⁻¹ per umol L⁻¹ AOU. This slope is steeper than the Redfield ratio slope (123/138 = 0.89), as proposed by (Xue and Cai 2020). which is based on conditions dominated by aerobic respiration and production. The steeper slope observed in the East Frisian WS suggests deviations from these typical conditions, indicating that the biogeochemical processes in this region may differ from those assumed in the Redfield model (Fig. 14). Variations in production and respiration, including Photosynthetic Quotient (PQ) and Respiratory Quotient (RQ) (Gazeau et al., 2005; Hopkinson and Smith, 2005), as well as the variability of the physiological status of different algae species (Wolfstein et al., 2000) could contribute to this deviation and can influence the observed slope. This may also be caused by specific local environmental conditions or deviating biogeochemical processes. Therefore, Xue and Cai (2020) assumed that this is due to higher tendency of dissolution of CaCO₃, which has been suggested as a and to determine the source for increasing TA (Norbisrath et al., 2023), where the authors assumed that TA was produced in the sediments through anaerobic processes and CaCO3 dissolution, and concluded that the Dutch Wadden Sea can be a potential source for TA (Norbisrath et al., 2023). This can contribute to TA generation in the East Frisian WS as well, especially in summer in the Western part. It has been hypothesized that TA generation within the Wadden Sea may have an important effect on the carbon storage capacity of the North Sea (Burt et al., 2016; Schwichtenberg et al., 2020) and thus on carbon dynamics, therefore the seasonal dynamics we observe can modulate this effect, and sink dynamics of carbon on such a large spatial and temporal scale (Table 4; Fig. 5). We successfully demonstrated that TA increased in the spring because of intense primary production, most likely driven by nitrate uptake (Figs. 5; Fig. 6), highlighting the impact of biological activity on carbonate system dynamics. During the other seasons, the system acted as a source of DIC, indicating seasonal shifts in carbon cycling. Similar patterns of intense production periods and TA increases have also been reported in the North Sea adjacent to the Wadden Sea (Voynova et al., 2019). Additionally, we observed TA production during summer, which was more prominent in the Western WS, further suggesting that these intertidal regions act as a stronger source of TA and DIC during all seasons except in spring, compared to the Eastern EFWS.

Figure 15 indicates a mix of the dominate processes of respiration and CO₂-uptake during this season. This can also be seen in the increasing *p*CO_{2 obs} concentrations (Fig. 4). However, when we analyze the nutrient content during this season, higher NO₃-concentrations were measured (Fig. 12; Fig. 13). Nitrification involves the conversion of NH₄+ to NO₂-, causing a decrease of TA by 2 moles per mole N, through the oxidation of ammonia to NO₂-. In addition, the nitrogen fixation could decrease TA by 1 mole per mole of N. The process consumes hydrogen ions (H+) and releases hydroxide ions (OH-), leading to an increase of pH (Brenner et al. 2016). This could indicate a possible mix of these processes in addition to respiration and CaCO₃ dissolution in March 2022, controlling the carbonate dynamics in the intertidal region of the East Frisian WS (Fig.15). In

October 2021, [TA-DIC] < 200 µmol kg⁻¹ are found, suggesting respiration and CO₂ release during this season (Fig. 14; Fig. 15). The uptake of CO₂ from the atmosphere by the ocean can increase DIC, but not TA, followed by a decreasing [TA-DIC] (Xue and Cai 2020).

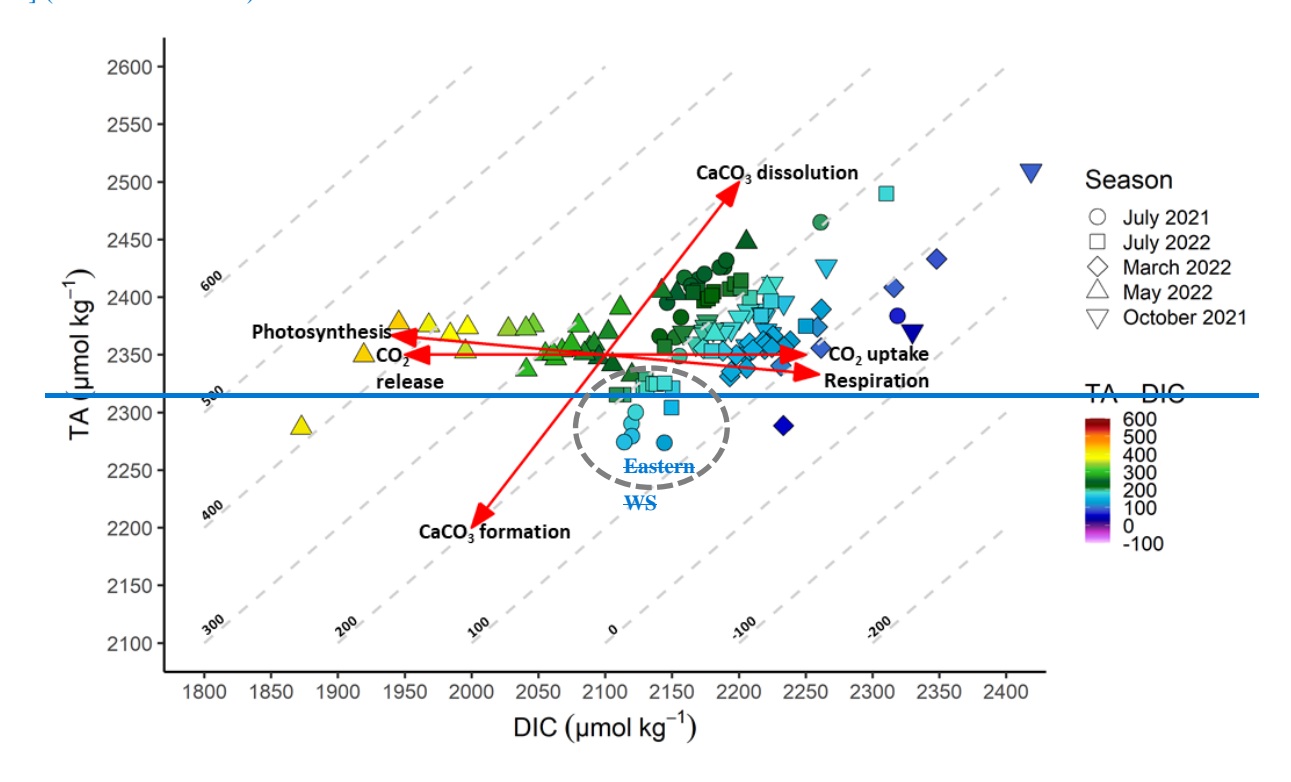


Figure 15: DIC versus TA plot from all seasons, with the colored value of [TA-DIC] in µmol kg⁻¹ from the intertidal region with 4.2 Seasonal TA Production and DIC Dynamics in the EFWS

670

675

680

The data reveal important differences in the patterns between years and regions in summer (Table 4; Fig. 2 – 5). The observed summer dynamics in the Eastern and Western EFWS show distinct patterns in the biogeochemical processes related to TA and DIC production. Positive ΔTA_{excess} (e.g., 123.0 ± 27.8 μmol kg⁻¹ in July 2021) and ΔDIC_{excess} (23.4 ± 27.6; Table 4) values suggest that there is excess of TA and DIC in the Western EFWS. One key biogeochemical process, which can contribute to increasing TA, without a proportional increase in DIC, is the dissolution of CaCO₃, which results in elevated [TA-DIC] values (>200 μmol kg⁻¹) (Chen and Wang, 1999; Hoppema, 1990). However, CaCO₃ dissolution can be ruled out as a major TA source in the water column, since calcite is supersaturated (Ωcal > 1) during the study period (Brasse et al., 1999; Norbisrath et al., 2024). Nevertheless, in the sediments large amount of DIC can be produced by carbonate shells and transported by erosion processes into the water column (Brasse et al., 1999). Previous studies have estimated that TA production in the Wadden Sea is driven by anaerobic processes such as denitrification and/or CaCO₃ dissolution in sediments (Norbisrath et al., 2024; Thomas et al., 2009). Anaerobic degradation of organic matter—via denitrification and sulfate reduction—releases both

TA and DIC (Brasse et al., 1999; Hu and Cai, 2011; Norbisrath et al., 2024; Thomas et al., 2009), with TA concentrations reaching up to 2310 µmol kg⁻¹ in summer (Thomas et al., 2009). Other studies suggest that permeable Janssand sediments (a tidal sand flat in the back-barrier area of Spiekeroog Island, Eastern EFWS) exhibit the highest potential denitrification rates (Gao et al., 2010).

685

690

695

700

705

710

715

In the summer months, the production of TA in both the Eastern and Western EFWS can be attributed to the decomposition of organic matter, especially following a productive spring season, such as the one observed in May 2022 (see section 4.3), which likely led to an elevated input of organic matter into the system (Borges et al., 2017). This organic matter subsequently undergoes both aerobic and anaerobic decomposition in the sediments during the summer months, where anaerobic processes like denitrification and sulphate reduction are drivers in generating both TA and DIC (Brasse et al., 1999; Norbisrath et al., 2024). These processes can significantly contribute to the enhancement of TA production (Fig. 4a, b; Fig. 5b), especially in the Western EFWS, where sedimentary anaerobic processes dominate in the summer (Al-Raei et al., 2009; Böttcher et al., 1998; Hu and Cai, 2011; Kamyshny and Ferdelman, 2010; Norbisrath et al., 2024; Thomas et al., 2009; Wu et al., 2015). Furthermore, with oxygen saturation remaining high (> 100 % saturation) and apparent oxygen utilization (AOU) being negative (Fig. 4a), it is evident that the water column is net autotrophic. This suggests that TA is primarily produced in the sediments and subsequently transported into the water column, rather than being generated in situ via remineralization (Beck and Brumsack, 2012; Postma, 1981).

Organic matter remineralization varies regionally across the North Frisian Wadden Sea (NFWS), EFWS, and Jade Bay (Van Beusekom et al., 2012; Kowalski et al., 2013). The NFWS favours aerobic degradation due to its wide tidal basins and highwater exchange (~8.1 km³ d⁻¹), resulting in lower organic matter accumulation, reduced eutrophication, and lower TA production relative to DIC (Van Beusekom et al., 2012; Kowalski et al., 2013; Schwichtenberg et al., 2020). In contrast, the EFWS experiences higher eutrophication and organic matter accumulation due to its narrower basins and limited exchange, promoting anaerobic degradation processes (e.g., sulfate reduction), which enhance TA production (Van Beusekom et al., 2012; Kowalski et al., 2013; Schwichtenberg et al., 2020; Thomas et al., 2009). Jade Bay, with the lowest water exchange (~0.8 km³ d⁻¹), exhibits sporadic high TA/DIC ratios, likely due to short-term iron reduction processes (Brasse et al., 1999). A similar pattern was also seen in the Eastern EFWS compared to the Western in [TA-DIC] dynamics (Fig. 2; Fig. 4b). In comparison to the Western, the Eastern EFWS consistently exhibits lower [TA-DIC] values (<200 μmol kg⁻¹) during the summer months of 2021 and 2022, while the Western EFWS shows slightly higher [TA-DIC] values (>200 umol kg⁻¹: Fig. 4b). This difference can be attributed to enhanced CaCO₃ formation, as indicated by its Ω cal (1.9 \pm 0.8) in the Eastern (Fig. 4b). CaCO₃ formation likely consumes TA (Chen, 1978), leading to the observed shift toward negative $\Delta TA_{\text{excess}}$ values (Fig. 5b). The formation of CaCO₃, particularly in sediments or shells, contributes to the lower observed source of TA in the Eastern compared to the Western WS. Despite this, the region still acts as a net source of TA, which aligns with the assumption that the Eastern EFWS can contribute TA to the coastal system during the summer months, especially from anaerobic degradation processes (Schwichtenberg et al., 2020; Thomas et al., 2009).

Additionally, the salinity 25-32.5. The isoclines are representing the [TA-DIC] values. The red lines showing the related biogeochemical processes (Photosynthesis, Respiration, CO₂ release and CO₂-uptake and CaCO₃-formation / dissolution), that could cause the changes in TA and DIC in the intertidal region of the intertidal East Frisian Wadden Sea. The Eastern part of the East Frisian is highlighted here with the dotted grey cycle.

720

725

730

735

740

745

750

Higher TA concentrations were found in summer, where compared to the North Sea, the TA concentrations in the WS were higher (> 2489 μ mol kg⁻¹), suggesting a generation of TA in the intertidal WS (Fig. 7, Fig. 8). In the summer (July 2021, July 2022), [TA DIC] values (< 200 μ mol kg⁻¹) from the Eastern WS are located under the respiration/photosynthesis line (Fig. 14; Fig. 15). In contrast, the measured [TA DIC] concentrations in the Western WS in summer are > 200 μ mol kg⁻¹ (Fig. 15), and above the respiration/photosynthesis fit.

Inchange observed in July 2022, the salinity in the same region changed by 2 3 units from one day (was likely due to local anthropogenic influences, such as the sluice opening in summer 2022. On July 11) to another (July 12), where the salinity was higher in the East (Fig. 2), leading to the slightly higher measured TA values (+53.7 ± 36.7 µmol kg⁻¹) in July 2022, compared to the previous year (Table 3). On the sampling day July 11, 2022, the sluice in Neuharlingersiel was opened just before we started our sampling. Due to this anthropogenic influence, it is reasonable to treat these July 11 measurements as anomalies, potentially influenced by the This anthropogenic intervention likely caused sudden changes in salinity and local hydrological conditions (Fig. S1; Fig. 3a, b), making it reasonable to treat the July 11 measurements as anomalous. It is important to note that the lower [TA-DIC] values in the Eastern EFWS are observed both on the day of sluice opening in July 2022 and on the day when the sluice was closed in July 2021. This suggests that the impact of the sluice opening did not have a major impact on the overall [TA-DIC] dynamics in the region. However, higher temperatures in summer also enhances evaporation, which could have an impact on TA and salinity, both would increase as a result (Schneider et al., 2007). A study by Onken and Riethmüller (2010), showed that evaporation in the tidal flats of the WS raised salinity by 0.65 within just 3.5 hours, indicating that tidal flats experience intensified evaporation during warmer months compared to other areas. This can also be seen in the stations with higher salinities (-32) of the Eastern intertidal WS, which can be identified with lower [TA DIC] (< 200 μmol kg⁻¹) values and the Western stations with lower salinity and thus slightly higher [TA DIC] values (Fig. 14; Fig. 15). Consequently, it is likely that CaCO₃ formation occurs in the Eastern WS, as indicated by its Ω cal of 1.9 \pm 0.8, while CaCO₃ dissolution is more prevalent in the Western part of the East Frisian WS, which has a Ωcal of 3.8 ± 0.4 (Fig. 15). This suggests a favorable environment for calcite formation in the Western WS, whereas the Eastern WS, while still supersaturated, may experience conditions that lean toward dissolution. CaCO₃ formation by 1 mole is known to decrease TA by 2 moles, changing [TA DIC] by 1 mole (Xue and Cai 2020). In contrast, as CaCO₃ dissolves, TA and DIC increases and [TA DIC] increases by 1 mole. The same regional variability is observed in July 2021 (Fig. 7, Fig.8), suggesting that CaCO₂ dissolution dominates and generates TA in the Western WS (Fig. 15). This TA generation in summer can change the buffer capacity, allowing for the Western WS to potentially take up or store carbon (Fig. 15) (Gruber et al., 2019; Li et al., 2024), compared to other seasons, and despite the southern North Sea being considered in general as a carbon source to the atmosphere (Thomas et al. 2009; Voynova et al. 2019). This also suggests that the intertidal regions of the Western Frisian WS can be a source of TA to the coast in the summer, as previously proposed by (Thomas et al. 2009; Voynova et al. 2019).

In contrast, These seasonal shifts in spring (May 2022)TA can influence the coastal ocean's ability to absorb carbon from the atmosphere (Burt et al., 2016; Gruber et al., 2019; Li et al., 2024; Schwichtenberg et al., 2020). In summer, the generation of TA and DIC may alter the region's buffering capacity, with the Western WS possibly storing or taking up carbon (Fig. 7) (Gruber et al., 2019; Li et al., 2024). These findings align with previous studies (Thomas et al., 2009; Voynova et al., 2019) suggesting that the intertidal regions of the EFWS act as a source of both TA and DIC to the coastal system during the summer months.

Particularly, the tidal WS plays an important role in the biogeochemical cycling of the North Sea (Santos et al., 2015; Thomas et al., 2009), because many European rivers empty in the WS (Thomas et al., 2009). A few studies discussed the generation in of TA in summer before (Schwichtenberg, 2013; Voynova et al., 2019), however in summer the riverine inflow is lowest, which could not explain an increase of TA in the WS. The highest riverine contribution of TA is expected from January to April (Pätsch and Lenhart, 2004; Schwichtenberg, 2013). The moderate rainfall and cooler-than-average weather in October 2021 may have influenced the hydrology of the region, potentially causing increased terrestrial runoff and enhanced delivery of alkalinity-rich water to the coastal system. The slight source of DIC in October (Table 3; Fig. 4d) suggests that organic matter remineralization and sediment-water exchange continue to play a role during this period (Borges et al., 2017). In addition, pore waters enriched with remineralized nutrients are actively released into the overlying water column (Beck and Brumsack, 2012) and organic matter-enriched water masses transported from the North Sea contribute to the availability of degradable material in the Wadden Sea, sustaining biogeochemical activity into autumn(Van Beusekom et al. 1999). This mechanism aligns with studies highlighting the importance of tidal-driven nutrient and carbon fluxes in permeable sediments (Postma, 1981), where advective transport processes facilitate the continuous exchange of dissolved carbon species between sediments and the water column (Santos et al., 2015).

4.3 Nitrate Assimilation and Carbonate Dynamics in Spring

755

760

765

770

The highesthigh rates of photosynthesis, suggested by were measured in our study in the spring of 2022 (May 2022). This is evidenced by high O₂ levels (up to 180 % saturation), low *p*CO₂*p*CO₂ obs₇ (Table 2) and high dissolved oxygen, pH and chlorophyll a levels, along with negative AOU values (Fig. 3; Fig. 4) (Artioli et al., 2012; Thomas et al., 2005b), result in a decrease in AOU (down to - 169 μmol L⁻¹) over the day (Table 2; Fig. 14) and an increased [TA DIC]₇; Fig. 4a) (Artioli et al., 2012; Thomas et al., 2005). These findings highlight the dominant role of photosynthetic activity in modulating the carbonate system, particularly in the Western EFWS, where carbon fixation via photosynthesis is a key factor in this study. The resulting changes in [TA-DIC] during this period are reflected in the AOU to [TA-DIC] relationship shown in Figure 4a, with a steeper negative slope of -1.416 μmol kg⁻¹ per μmol L⁻¹ AOU, deviating from the Redfield ratio of -0.89 (Xue and Cai, 2020). This deviation suggests that the EFWS may differ from the typical conditions assumed in the Redfield model (Redfield et al., 1963), which is primarily based on aerobic respiration and production (Xue and Cai, 2020).

<u>Furthermore, [TA-DIC] increased</u> due to the <u>substantial drawdown of significant decrease in DIC</u> in May 2022 (Fig. 6; 4b). Together with the positive ΔTA_P and strongly negative ΔDIC_{excess} values after removal of mixing, this supports the findings of

intense spring primary production generating TA, while drawing down DIC (Fig. 13; Fig. 14). This indicates that this region is a 5). This was particularly evident in the Western EFWS, but also in the Eastern, indicating the Western EFWS is a stronger sink for CO₂ due to carbon fixation and nitrate assimilation(Borges et al., 2005). A decline of AOU can significantly change the DIC concentration and consequently increase [TA-DIC] values, which was the case during the productive seasons (July 2021, July 2022, May 2022).

790

800

805

810

815

Strong biological production reduced DIC concentrations, indicating consumption of inorganic carbon with DIC falling below to the mixing line (Fig. 8), and *p*CO_{2 obs} reaching levels of < 200 μatm (Fig. 4). This can also be seen in Fig. 14, where the (Borges et al., 2005). The May measurements follow roughly the photosynthesis/respiration line, indicated by the progressively low DIC values in May (Fig. 7). At the same time, TA also increased slightly during this period, as indicated by the both regions, and slight deviation from the photosynthesis/respiration line (Fig. 14), increasing increase in TA (9.1 ± 29.2 μmol kg⁻¹ from March 2022 to May 2022-by approximately 9.1 ± 29.2 μmol kg⁻¹ in the intertidal regions, Fig. 4b), above the mixing line (Fig. 8). This suggests a slight production of TA compared to March 2022.3b). The relationship in Fig. 12Figure 6 also indicates that primary production is influenced by nitrate and silicate availability. Overall, the data confirm that Nitrate concentrations decreased substantially from 65 μmol kg⁻¹ in March to 22 μmol kg⁻¹ in May 2022 (Fig. 6; Fig. S4), coinciding with the period of intense primary production. This significant drawdown in nitrate concentrations suggests that nitrate assimilation was the primary driver of the observed decrease in DIC and the slight increase in TA during this period. Nitrate assimilation involves the consumption of hydrogen ions (H⁺) and the release of hydroxide ions (OH⁻), which leads to an increase in pH and, consequently, in TA (Brenner et al., 2016; Wolf-Gladrow et al., 2007). Therefore, nitrate assimilation played a crucial role in shaping the carbonate system dynamics by decreasing CO₂ and DIC, while increasing TA.

The regression analysis of ΔNO₃⁻ and ΔDIC between March and May 2022 revealed a slope of 6.90 for the changes in nitrate concentrations (Fig. 6), which is close to the Redfield ratio of 6.625 for the C:N ratio (Redfield et al., 1963). This close match suggests nitrate assimilation during the spring bloom, which is closely linked to a reduction in DIC. Similarly, the ΔSiO₂ regression produced a slope of 8.11 (Fig. 6), which is also close to the Redfield ratio for SiO₂ (7.067), further supporting the conclusion that the enhanced primary production leads to a significant decrease in DIC, which is reflected in the changes in in this region during the spring bloom contributed to nutrient concentrations, as well as a slight production of TA (Fig. 7; Fig. 8; Fig. 13)-uptake, particularly nitrate and silicate.

We therefore propose that assimilation of NO_3^- during the time of intense primary production in May 2022 could explain the local increase of total alkalinity during the spring bloom. First, the maximum concentration of NO_3^- was captured in March before the high biologically productive season started in May 2022 (Fig. 11–154 - 7), with maximum concentrations measured in the Western WS. A significant drawdown of NO_3^- in the intertidal regions from the maximum value of 65 μ mol kg⁻¹ in March 2022 to 22 μ mol kg⁻¹ in May 2022, resulted in an average decrease of 19.2 \pm 9.6 μ mol kg⁻¹ of NO_3^- (Fig. 12; Fig. 13). 6; Fig. S4). Brewer and Goldman (1976) also documented that nitrate assimilation increases TA (9.1 \pm 29.2 μ mol kg⁻¹).

An uptake of NH_4^+ was not obvious, because NH_4^+ concentrations were much lower during this period (Fig. 12S4), suggesting only a small impact on TA patterns. In contrastTherefore, the limited influence of NH_4^+ uptake further emphasizes the central

role of nitrate assimilation in shaping the observed patterns in the carbonate system. Nitrification, the process by which NH₄⁺ is converted into NO₂⁻, causes a decrease of NO₃ in TA by 2 moles per mole of nitrogen (Wolf-Gladrow et al., 2007; Xue and Cai, 2020), thus has the opposite effect compared to nitrate assimilation, which increases TA. The decrease in NO₃⁻ from May 2022 to July 2022 was smaller in comparisonless pronounced (1.51 ± ± 5.16 μmol kg⁻¹; Fig. 12). However, generally the NO₃⁻ concentration is low in 6), which is consistent with the general trend of lower NO₃⁻ concentrations in summer, which was due to likely driven by higher turnover rates (Kieskamp et al. 1991). Since denitrification is dependent on nitrate supply, previous studies identified lower denitrification rates seasonally in summer (Kieskamp et al. 1991; Faber et al. 2014). Due to the high oxygen concentrations in the intertidal East Frisian WS, anaerobic denitrification, which can increase TA (Chen and Wang, 1999), is unlikely in the water column, but can take place in the sediments (not addressed in this study)..., 1991).

4.3 Biological and thermal pCO₂ dynamics

820

825

835

840

845

850

Previous work demonstrated that the most 5 Conclusion

The findings highlight significant temporal variability in the ocean surface pCO₂ is seasonal, linked to either thermal or non-thermal factors (Takahashi et al., 1993, 2002). The pCO₂ changes approximately 4.2 % for every 1°C change in temperature, increasing with warmer sea surface temperature (SST) and decreases with colder SST (Takahashi et al., 1993).

Seasonal changes in the observed, biological and thermal components of pCO₂ were observed in the East Frisian WS in the

Eastern and Western WS (Fig. 5). The temperature on March 2022 was low (3.89 – 6.47 °C) (Fig. 2), reducing the solubility of *p*CO₂ (Prowe et al. 2009). This was also the season in which the lowest *p*CO_{2 therm} (453 μatm) was measured (Fig. 6). The biological component of pCO_{2 bio} was relatively high in comparison (see section 3.1.2). However, the NO₃-concentration

measured in March 2022 was also higher (Fig. 12) in comparison.

Especially in May 2022, low *p*CO_{2 obs} values (down to 141.3 μatm) close to the calculated *p*CO_{2 obs} values were measured (Fig. 6), suggesting a biological control of primary producers. The average measurement of *p*CO_{2 obs} agrees seasonally well with other studies in the North Sea (Prowe et al. 2009; Macovei et al. 2021), where *p*CO_{2 obs} dropped constantly during spring season and increased during early summer (Fig. 6). The *p*CO_{2 obs} and DIC decreased, as a result of the production of organic matter by primary producers (Macovei et al. 2021) in May 2022 (Fig. 4; Fig. 6). In contrast, in July 2022, an increase in *p*CO₂ was observed, attributed to the remineralization of organic material (Macovei et al. 2021; Artioli et al. 2012), but also an increase in surface water temperatures in July (Fig. 6). During remineralization, organic matter is broken down, releasing CO₂. Simultaneously, the data show that Ωcal was relatively high (Table 2; Fig. 5). Additionally, lower DIC concentrations were measured, which could indicate enhanced primary production or another CO₂ consuming process. Similar results were also found in previous studies, which defines thermal effects, reduced mixing, remineralization and CO₂ uptake by phytoplankton as possible drivers of seasonal high *p*CO₂ observed in the North Sea in summer (Prowe et al. 2009).

Lower salinity water masses (> 25) contained higher pCO_{2 obs} concentrations during all seasons, which suggests a possible riverine input of higher pCO₂ water mass coming from the Ems and Weser River estuaries (Fig. 2), especially in the wet

seasons. Regionally, the measured $pCO_{2 \text{ obs}}$ was low in the intertidal East Frisian WS compared to the high turbid Ems River estuary in summer (July 2021, July 2022, May 2022). Previous studies also found this pattern of lower salinity water masses related to pCO_2 -concentrations with increase pCO_2 -concentrations where water masses of runoff enter the North Sea (Burt et al. 2016; Thomas et al. 2005a).

4.4 Additional Factors affecting TA and DIC Dynamics

855

860

865

870

875

880

Particularly, the tidal WS plays an important role in the biogeochemical cycling of the North Sea (Santos et al., 2015; Thomas et al., 2009), because many European rivers empty in the WS (Thomas et al. 2009). A few studies discussed the generation in of TA in summer before (Schwichtenberg, 2013; Voynova et al., 2019), however in summer the riverine inflow is lowest, which could not explain an increase of TA in the WS.

This observation is supported by the ΔTA_{excess} values, where the riverine mixing effect was removed (Fig. 10), showing a similar pattern as the mixing plots in summer in the Western WS (Fig. 8). Nonetheless, the TA values measured in March 2022 and the ΔTA_{excess} (Fig. 8; Fig. 10) values indicating a mixing effect of riverine water masses coming from the Ems River estuary (Fig. 10), due to the inconsistency in comparison to the mixing plots (Fig. 8c). The highest riverine contribution of TA is expected from January to April (Pätsch and Lenhart, 2004; Schwichtenberg, 2013). However, the moderate rainfall and cooler than average weather in October 2021 may have influenced the hydrology of the region, potentially causing increased terrestrial runoff and enhanced delivery of alkalinity rich water to the coastal system. This would contrast with drier, warmer periods, where evaporation and lower river discharge would dominate (Onken and Riethmüller, 2010).

The tidal dynamics of the WS can also play a crucial role in regulating biogeochemical processes. The tidal flats may experience intensified cycling of carbonates, particularly in transitional seasons like autumn when temperature and biological activity are still relatively high. This could contribute to an accumulation of TA in the system (Thomas et al., 2009). Internal processes within the WS, such as carbonate dissolution or sediment reworking, could also explain the higher TA values (Brenner et al., 2016; Burt et al., 2014; Van Dam et al., 2022; Norbisrath et al., 2023; Thomas et al., 2009). These processes may be more pronounced in autumn as biological and chemical activity shifts with the changing seasons. Previous studies, like Schwichtenberg (2013), suggest that riverine loads account for only about 9% of TA variability in the German Bight. However, localized weather events and specific regional conditions in autumn might enhance the riverine contribution during certain periods.

Previous studies (Hoppema, 1990; Norbisrath et al., 2023) have observed an increase in TA and DIC from high to low tide over a tidal cycle in the Wadden Sea. However, this study could not sample all stations during low tide, so it is not possible to capture the complete tidal patterns here. This means that some of the results might be affected by tidal changes, with an average increase of 51.6 μmol kg⁻¹ in TA and 101.3 μmol kg⁻¹ in DIC during ebb tide, as proposed before (Norbisrath et al., 2023). In contrast, the Ωeal was highest at high tide (3.8) and lowest at ebb tide (3.1) in the Dutch Wadden Sea (Norbisrath et al., 2023). The intertidal East Frisian WS in this study was mostly sampled during low or rising tide, whereas the stations more offshore (behind the Islands) and the stations in the Jade Bay (Fig. 1) mostly were sampled during high tide. The stations in the Western part of the East Frisian WS were mainly sampled during rising tide during all seasonal cruises. However, a slight variation in

sampling times could not be avoided, which may explain some of the observed TA dynamics in the Western WS, particularly the increased influence of sediments at low tides (Norbisrath et al., 2023). Therefore, CaCO₃ dissolution at the water sediment interface, where TA is remineralized (Norbisrath et al., 2023) could be an important driver for these dynamics. The transect from Norddeich harbour to Norderney, sampled during ebb or declining tide across all seasons, also exhibited notable patterns in TA and DIC, potentially influenced by tidal changes. Therefore, the higher TA and DIC values observed (Table 3; Fig. 7), particularly in October 2021, may be linked to sediment interaction and carbonate dissolution, highlighting the crucial role of tidal and sedimentary dynamics (Norbisrath et al., 2023) in shaping these biogeochemical parameters.

5 Conclusions

885

890

895

900

905

910

915

This study highlights the regional and seasonal variations in the EFWS carbonate system of the East Frisian Wadden Sea. reflecting on the broader carbon dynamics of in coastal and shelf seas. The findings reveal that both total alkalinity (TA) and dissolved inorganic carbon (DIC) vary substantially across different Both TA and DIC exhibit substantial variations across regions and seasons, with a notable decrease in DIC from East to West and an increase in TA during biologically productive periods, such as spring and summer. In spring 2022, a significant drawdown of NO₃⁻NO₃⁻ was observed, correlating with a slight increase in TA, likely due to nitrate assimilation during primary production. The generation of TA in the Western East Frisian Wadden Sea, particularly in summer, suggests that this region may play a role in carbon storage. The higher TA concentrations observed in summer, coupled with the processes of CaCO3 dissolution, indicate that the Western WS could act as a source of TA to the adjacent coastal waters. This TA generation may enhance the region's capacity to absorb CO₂, despite the broader southern North Sea generally being considered a carbon source to the atmosphere. Analyzing changes in ATA excess? ADIC_{access} and ATA_P helps better understand seasonal patterns and the underlying biogeochemical processes and mixing. The riverine input—which could have been a possible driver for TA production in the tidal driven East Frisian Wadden Sea—was excluded as a dominate reason, due to the low riverine input during the warm seasons. Nevertheless, higher inputs of riverine water masses can strongly influence TA and DIC in coastal regions and should not be ignored in such studies, like in March 2022 in this study. Primary production in May 2022 could explain up to 80 % of the ΔDIC_{excess} in the Western WS and up to 90 % ADICenses in the Eastern WS, which resulted in such an extreme drop in DIC, slight production in TA and drawdown in NO_3 -during this period. Primary production could explain up to 88 % of the ΔDIC_{excess} in the Western WS and up to 92 % in the Eastern WS, contributing to the significant drop in DIC, slight TA production, and NO₃⁻ drawdown during this period. The results of In the present study successfully applied summer, it is likely that the parameter fremineralization of organic matter, combined with the dissolution of CaCO₃ in sediments, contributes to higher TA production, especially in the coastal and nearshore areas of the Western EFWS. On the other hand, the Eastern EFWS may experience greater CaCO₃ formation, which may reduce TA levels ([TA-DIC] to explain seasonal and regional changes in TA < 200 µmol kg⁻¹). However, the region still acts as a net source of TA, in part due to the known high rates of benthic anaerobic respiration, such as organic matter decomposition and DIC in the East Frisian Wadden associated TA production, particularly after the high productivity of the spring season. This TA generation may enhance the region's capacity to absorb CO2, despite the broader southern North Sea eaused by generally being considered a carbon source to the atmosphere. These findings emphasize the complexity of the biogeochemical processes in a coastal system. Understanding the described biogeochemical dynamics is crucial for predicting the impact of climate change on coastal and shelf seas, where driving regional and seasonal variability in TA and DIC can influence the regional carbon cycling and contribute to broader oceanic carbon dynamics. However, in a tidal system such as the East Frisian Wadden Sea, additional factors such as nutrient loading, groundwater discharge, riverine input, tides as well as sediment pelagic coupling should also considered.

The observed regional and seasonal variability in the the EFWS carbonate system of the East Frisian Wadden Sea reveals complex biogeochemical processes that are, particularly those influenced by tidal cycles, riverineriver inputs, and sediment interactions. These dynamics highlight the regional and seasonal factors when assessing the carbonate capacity and carbon dynamics of coastal ecosystems like the Wadden Sea. Tidal variations, though not fully captured in the study, significantly impact TA and DIC concentrations, with ebb tides typically showing higher levels due to sediment interactions and CaCO3 dissolution. Riverine inputs, particularlyespecially from the Ems River estuary, also shape the influence local carbonate chemistry, though. However, the relatively low summerriver inflows during the summer suggest that sediment interactions processes, such as organic matter decomposition, may play a largermore dominant role.

To fully understandgain a comprehensive understanding of these intricate interactions and their implications for impact on carbon storage and marine biogeochemistry in this ecologically significant region, further research, including sediment studies and continuous tidal monitoring, is essential. This study is the first to combine the analysis of [TA-DIC] with other parameters such as ΔTA_{excess}, ΔDIC_{excess}, and ΔTA_P to infer underlying biogeochemical processes - such as biological productivity and nutrient availability. This innovative approach offers a new way to examine how various environmental factors interact and influence the carbonate system. The results have the potential to refine existing models of the biogeochemical cycle, providing valuable insights for more accurate climate predictions and improved strategies for managing coastal systems in response to environmental change.

940 Code and data availability

920

925

930

935

The data supporting our findings withinin this study have been submitted by Lara Luitjens (NLWKN) to the PANGAEA data repository and are currently undergoing final editorial processing. A DOI for the dataset will be available upon completion of the review process. (Luitjens et al., in review). The datasets can be accessed through the following links: https://doi.pangaea.de/10.1594/PANGAEA.974424

945 https://doi.pangaea.de/10.1594/PANGAEA.974426

https://doi.pangaea.de/10.1594/PANGAEA.974427

https://doi.pangaea.de/10.1594/PANGAEA.974428

Competing interests

The contact author has declared that none of the authors has any competing interests.

950 Acknowledgements

955

960

965

975

We deeply appreciate the laboratory technicians We thank Martina Gehrung, Tanja Pieplow and Catharina Petrauskas for their exceptional technical support, meticulous work and dedication. They ensured the reliability and accuracy of our data through their careful handling of samples and precise analytical measurements. The scientists and crew who participated in the research expeditions, including the captain Alexander Heidenreich and the crew of the *RV Burchana* (Jens Voß and Winfried Bruns) are also greatly appreciated. It was their hard work, professionalism and co-operation during the challenging field work that made it possible to collect the data required for this study. The success of our research would not have been possible without your tireless efforts at sea. We thank all of you for your unwavering support and commitment.

Finally, we would like to acknowledge the support and valuable discussions with the members of the "CARBOSTORE" project and especially <u>Prof.</u> Dr. habil. Michael Böttcher from the Institute for Baltic Sea Research in Warnemünde (Germany).

The author wishes to express their gratitude to the anonymous reviewer for their constructive comments and valuable feedback, which significantly enhanced the manuscript.

Financial support

This research was funded through the "CARBOSTORE" project (Grant Number 03F0875A), by the German Federal Ministry of Education and Research (BMBF). Additionally, the Helmholtz-Zentrum Hereon covered the article processing charges for this open-access publication.

References

4H - Jena engineering GmbH: Data Processing for CONTROS HydroC⊕ ® CO2 (Manual), 1–7 pp.. 2021.

Abril, G., Etcheber, H., Delille, B., Frankignoulle, M., and Borges, A. V.: Carbonate dissolution in the turbid and eutrophic Loire estuary, Mar Ecol Prog Ser, 259, 129–138, https://doi.org/10.3354/meps259129, 2003.

- Al-Raei, A. M., Bosselmann, K., Böttcher, M. E., Hespenheide, B., and Tauber, F.: Seasonal dynamics of microbial sulfate reduction in temperate intertidal surface sediments: controls by temperature and organic matter, Ocean Dyn, 59, 351–370, https://doi.org/10.1007/s10236-009-0186-5, 2009.
 - Artioli, Y., Blackford, J. C., Butenschön, M., Holt, J. T., Wakelin, S. L., Thomas, H., Borges, A. V., and Allen, J. I.: The carbonate system in the North Sea: Sensitivity and model validation, Journal of Marine Systems, 102–104, 1–13, https://doi.org/10.1016/j.jmarsys.2012.04.006, 2012.

- Bauer, J. E., Cai, W. J., Raymond, P. A., Bianchi, T. S., Hopkinson, C. S., and Regnier, P. A. G.: The changing carbon cycle of the coastal ocean, Nature, 504, https://doi.org/10.1038/nature12857, 2013.
- Beck, M. and Brumsack, H. J.: Biogeochemical cycles in sediment and water column of the Wadden Sea: The example Spiekeroog Island in a regional context, Ocean Coast Manag, 68, 102–113, https://doi.org/10.1016/j.ocecoaman.2012.05.026, 2012.

985

995

- Van Beusekom, J. E. E. and De Jonge, V. N.: Long-term changes in Wadden Sea nutrient cycles: Importance of organic matter import from the North Sea, Hydrobiologia, 475–476, 185–194, https://doi.org/10.1023/A:1020361124656, 2002.
- Blackford Van Beusekom, J. E. E., C.Brockmann, U. H., Hesse, K.-J., Hickel, W., Poremba, K., and Gilbert, F. J.: pH variability and CO₂ induced acidification Tillmann, U.: The importance of sediments in the transformation and turnover of nutrients and organic matter in the Wadden Sea and German Bight, Deutsche Hydrographische Zeitschrift, 51, 245–266, https://doi.org/10.1007/BF02764176, 1999.
- <u>Van Beusekom, J. E. E., Buschbaum, C., and Reise, K.: Wadden Sea tidal basins and the mediating role of the North Sea-Journal of Marine Systems, 64, 229–241 in ecological processes: scaling up of management?, Ocean Coast Manag, 68, 69–78, https://doi.org/10.1016/j.imarsys.2006.03.016, 2007ocecoaman.2012.05.002, 2012.</u>
- Borges, A. V., Schiettecatte, L.-S., Abril, G., Delille, B., and Frankignoulle and Gazeau, F.: Carbon dioxide in European coastal waters, Estuar Coast Shelf Sci, 70, 375–387, https://doi.org/10.1016/j.ecss.2006.05.046, 2006.
 - Borges, A. V., Speeckaert, G., Champenois, W., Scranton, M.: Budgeting sinks, I., and sourcesGypens, N.: Productivity and Temperature as Drivers of CO₂Seasonal and Spatial Variations of Dissolved Methane in the coastal ocean: Diversity of ecosystem counts, Geophys Res Lett 32, 1 4Southern Bight of the North Sea, Ecosystems, 21, 583–599, https://doi.org/10.1029/2005GL023053, 20051007/s10021-017-0171-7, 2017.
 - Böttcher, M. E., Oelschläger, B., Höpner, T., Brumsack, H. J., and Rullkötter, J.: Sulfate reduction related to the early diagenetic degradation of organic matter and "black spot" formation in tidal sandflats of the German Wadden Sea (southern North Sea): Stable isotope (¹³C, ³⁴S, ¹⁸O) and other geochemical results, Org Geochem, 29, 1517–1530, https://doi.org/10.1016/S0146-6380(98)00124-7, 1998.
- Brasse, S., Reimer, A., Seifert, R., and Michaelis, W.: The influence of intertidal mudflats on the dissolved inorganic carbon and total alkalinity distribution in the German Bight, southeastern North Sea, Journal of Sea Research, 93–103 pp., 1999.
 - Brenner, H., Braeckman, U., Le Guitton, M., and Meysman, F. J. R.: The impact of sedimentary alkalinity release on the water column CO₂ system in the North Sea, Biogeosciences, 13, 841–863, https://doi.org/10.5194/bg-13-841-2016, 2016.
 - Brewer, P. G. and Goldman, J. C.: Alkalinity changes generated by phytoplankton growth, Limnol Oceanogr, 21, 108–117, https://doi.org/10.4319/lo.1976.21.1.0108, 1976.
 - Burt, W. J., Thomas, H., Pätsch, J., Omar, A. M., Schrum, C., Daewel, U., Brenner, H., and De Baar, H. J. W.: Radium isotopes as a tracer of sediment water column exchange in the North Sea, Global Biogeochem Cycles, 28, 786 804, https://doi.org/10.1002/2014GB004825, 2014.

- Burt, W. J., Thomas, H., Hagens, M., Pätsch, J., Clargo, N. M., Salt, L. A., Winde, V., and Böttcher, M. E.: Carbon sources in the North Sea evaluated by means of radium and stable carbon isotope tracers, Limnol Oceanogr, 61, 666–683, https://doi.org/10.1002/lno.10243, 2016.
 - Cai, W. J., Hu, X., Huang, W. J., Jiang, L. Q., Wang, Y., Peng, T. H., and Zhang, X.: Alkalinity distribution in the western North Atlantic Ocean margins, J Geophys Res Oceans, 115, https://doi.org/10.1029/2009JC005482, 2010.
- Cao, Z., Dai, M., Zheng, N., Wang, D., Li, Q., Zhai, W., Meng, F., and Gan, J.: Dynamics of the carbonate system in a large continental shelf system under the influence of both a river plume and coastal upwelling, J Geophys Res Biogeosci, 116, https://doi.org/10.1029/2010JG001596. 2011.
 - Chen, C. T. A. and Wang, S. L.: Carbon, alkalinity and nutrient budgets on the East China Sea continental shelf, J Geophys Res Oceans, 104, 20675–20686, https://doi.org/10.1029/1999ic9000551999JC900055, 1999.
 - Chen, C.-T. A.: Decomposition of Calcium Carbonate and Organic Carbon in the Deep Oceans, Science, (1979), 201, 735–736, https://doi.org/10.1126/science.201.4357.735, 1978.

- Chierici, M., Fransson, A., and Nojiri, Y.: Biogeochemical processes as drivers of surface fCO₂ in contrasting provinces in the subarctic North Pacific Ocean, Global Biogeochem Cycles, 20, https://doi.org/10.1029/2004GB002356, 2006.
- Van Dam, B. R., Crosswell, J. R., Anderson, I. C., and Paerl, H. W.: Watershed Scale Drivers of Air Water CO₂ Exchanges in Two Lagoonal North Carolina (USA) Estuaries, Journal of Geophysical Research: Biogeosciences, 123, 271–287, https://doi.org/10.1002/2017JG004243, 2018.
- Van Dam, B., Lehmann, N., Zeller, M. A., Neumann, A., Pröfrock, D., Lipka, M., Thomas, H., and Böttcher, M. E.: Benthic alkalinity fluxes from coastal sediments of the Baltic and North seas: comparing approaches and identifying knowledge gaps, Biogeosciences, 19, 3775–3789, https://doi.org/10.5194/bg-19-3775-2022, 2022.
- Dickson, A. G.: An exact definition of total alkalinity and a procedure for the estimation of alkalinity and total inorganic carbon from titration data, Deep Sea Research Part A. Oceanographic Research Papers, 28, 609–623, https://doi.org/10.1016/0198-0149(81)90121-7, 1981.
 - Dickson, A. G., Afghan Duan, L., Song, J.-D., Li, X., Yuan, H., and Anderson, G. C.: Reference materials for oceanic CO₂ analysis: a method for the certification Zhuang, W.: Potential risks of total alkalinity, Mar Chem, 80, 185–197 CO₂ removal project based on carbonate pump to marine ecosystem, https://doi.org/10.1016/S0304-4203(02)00133-0, 2003.
- O35 Dickson, Aj.scitotenv.2022.160728, 1 March 2023, G., Sabine, C. L., Christian, J. R., and North Pacific Marine Science Organization.: Guide to best practices for ocean CO₂ measurements, North Pacific Marine Science Organization, 2007.
 - Faber, P. A., Evrard, V., Woodland, R. J., Cartwright, I. C., and Cook, P. L. M.: Pore water exchange driven by tidal pumping causes alkalinity export in two intertidal inlets, Limnol Oceanogr, 59, 1749–1763, https://doi.org/10.4319/lo.2014.59.5.1749, 2014.
- Feely, R., Doney, S., and Cooley, S.: Ocean Acidification: Present Conditions and Future Changes in a High-CO₂ World, Oceanography, 22, 36–47, https://doi.org/10.5670/oceanog.2009.95, 2009.

- Friedlingstein, P., O'Sullivan, M., Jones, M. W., Andrew, R. M., Bakker, D. C. E., Hauck, J., Landschützer, P., Le Quéré, C., Luijkx, I. T., Peters, G. P., Peters, W., Pongratz, J., Schwingshackl, C., Sitch, S., Canadell, J. G., Ciais, P., Jackson, R. B., Alin, S. R., Anthoni, P., Barbero, L., Bates, N. R., Becker, M., Bellouin, N., Decharme, B., Bopp, L., Brasika, I. B. M., Cadule, P., Chamberlain, M. A., Chandra, N., Chau, T.-T.-T., Chevallier, F., Chini, L. P., Cronin, M., Dou, X., Enyo, K., Evans, W., Falk, S., Feely, R. A., Feng, L., Ford, D. J., Gasser, T., Ghattas, J., Gkritzalis, T., Grassi, G., Gregor, L., Gruber, N., Gürses, Ö., Harris, I., Hefner, M., Heinke, J., Houghton, R. A., Hurtt, G. C., Iida, Y., Ilyina, T., Jacobson, A. R., Jain, A., Jarníková, T., Jersild, A., Jiang, F., Jin, Z., Joos, F., Kato, E., Keeling, R. F., Kennedy, D., Klein Goldewijk, K., Knauer, J., Korsbakken, J. I., Körtzinger, A., Lan, X., Lefèvre, N., Li, H., Liu, J., Liu, Z., Ma, L., Marland, G., Mayot, N., McGuire, P. C., McKinley, G. A., Meyer, G., Morgan, E. J., Munro, D. R., Nakaoka, S.-I., Niwa, Y., O'Brien, K. M., Olsen, A., Omar, A. M., Ono, T., Paulsen, M., Pierrot, D., Pocock, K., Poulter, B., Powis, C. M., et al.: Global Carbon Budget 2023, Earth Syst Sci Data, 15, 5301–5369, https://doi.org/10.5194/essd-15-5301-2023, 2023.
 Batth Syst Sci Data, 15, 5301–5369, https://doi.org/10.5194/essd-15-5301-2023, 2023.
- O55 Gao, H., Schreiber, F., Collins, G., Jensen, M. M., Kostka, J. E., Lavik, G., De Beer, D., Zhou, H. Y., and Kuypers, M. M. M.:

 Aerobic denitrification in permeable Wadden Sea sediments, ISME Journal, 4, 417–426,

 https://doi.org/10.1038/ismej.2009.127, 2010.
 - Gattuso, J. P., Frankignoulle, M., and Wollast, R.: Carbon and carbonate metabolism in coastal aquatic ecosystems, Annu Rev Ecol Syst, 29, 405–434, https://doi.org/10.1146/annurev.ecolsys.29.1.405, 1998.
- Gazeau, F., Borges, A., Barrón, C., Duarte, C., Iversen, N., Middelburg, J., Delille, B., Pizay, M., Frankignoulle, M., and Gattuso, J.: Net ecosystem metabolism in a micro-tidal estuary (Randers Fjord, Denmark): evaluation of methods, Mar Ecol Prog Ser, 301, 23–41, https://doi.org/10.3354/meps301023, 2005.
 - Grasshoff, K., Kremling, K., and Ehrhardt, M.: Methods of Seawater Analysis, edited by: Grasshoff, K., Kremling, K., and Ehrhardt, M., Wiley, https://doi.org/10.1002/9783527613984, 1999.
- Gruber, N., Clement, D., Carter, B. R., Feely, R. A., van Heuven, S., Hoppema, M., Ishii, M., Key, R. M., Kozyr, A., Lauvset, S. K., Lo Monaco, C., Mathis, J. T., Murata, A., Olsen, A., Perez, F. F., Sabine, C. L., Tanhua, T., and Wanninkhof, R.:

 The oceanic sink for anthropogenic CO₂ from 1994 to 2007, Science, (1979), 363, 1193–1199, https://doi.org/10.1126/science.aau5153, 2019.
- Grunwald, M., Dellwig, O., Beck, M., Dippner, J. W., Freund, J. A., Kohlmeier, C., Schnetger, B., and Brumsack, H. J.:

 Methane in the southern North Sea: Sources, spatial distribution and budgets, Estuar Coast Shelf Sci, 81, 445–456, https://doi.org/10.1016/j.ecss.2008.11.021, 2009.

Hopkinson, C. S. Herrling, G. and Smith, E. M.: Estuarine respiration: an overview of benthic, pelagic, Winter, C.: Tidally- and wholewind-driven residual circulation at the multiple-inlet system respiration, in: Respiration in Aquatic Ecosystems, Oxford University Press, 122 146East Frisian Wadden Sea, Cont Shelf Res, 106, 45–59, https://doi.org/10.1093/aeprof:oso/9780198527084.003.0008, 20051016/j.csr.2015.06.001, 2015.

- Hoppema, J. M. J.: The distribution and seasonal variation of alkalinity in the Southern Bight of the North Sea and in the Western Wadden Sea, Netherlands Journal of Sea Research, 26, 11–23, https://doi.org/10.1016/0077-7579(90)90053-J, 1990.
- Hu, X. and Cai, W. J.: An assessment of ocean margin anaerobic processes on oceanic alkalinity budget, Global Biogeochem

 Cycles, 25, https://doi.org/10.1029/2010GB003859, 2011.
 - Jiang, L. Q., Cai, W. J., and Wang, Y.: A comparative study of carbon dioxide degassing in river- and marine-dominated estuaries, Limnol Oceanogr, 53, 2603–2615, https://doi.org/10.4319/lo.2008.53.6.2603, 2008.
 - Joesoef, A., Huang, W. J., Gao, Y., and Cai, W. J.: Air-water fluxes and sources of carbon dioxide in the Delaware Estuary: Spatial and seasonal variability, Biogeosciences, 12, 6085–6101, https://doi.org/10.5194/bg-12-6085-2015, 2015.
- Kamyshny, A. and Ferdelman, T. G.: Dynamics of zero-valent sulfur species including polysulfides at seep sites on intertidal sand flats (Wadden Sea, North Sea), Mar Chem, 121, 17–26, https://doi.org/10.1016/j.marchem.2010.03.001, 2010.
 - Kieskamp, W., Lohse, L., Epping, E., and Helder, W.: Seasonal variation in denitrification rates and nitrous oxide fluxes in intertidal sediments of the western Wadden Sea, Mar Ecol Prog Ser, 72, 145–151, https://doi.org/10.3354/meps072145, 1991.
- Kowalski, N., Dellwig, O., Beck, M., Gräwe, U., Neubert, N., Nägler, T. F., Badewien, T. H., Kitidis, VBrumsack, H.-J., van Beusekom, J. E. E., and Böttcher, M. E.: Pelagic molybdenum concentration anomalies and the impact of sediment resuspension on the molybdenum budget in two tidal systems of the North Sea, Geochim Cosmochim Acta, 119, 198–211, https://doi.org/10.1016/j.gca.2013.05.046, 2013.
 - "Shutler, J. D., Ashton, I., Warren, M., Brown, I., Findlay, H., et. Al.: Winter weather controls net influx of atmospheric CO₂ on the north west European shelf, Sci Rep, 9, https://doi.org/10.1038/s41598-019-56363-5, 2019.

- Kroeker, K. J., Kordas, R. L., Crim, R., Hendriks, I. E., Ramajo, L., Singh, G. S., Duarte, C. M., and Gattuso, J. P.: Impacts of ocean acidification on marine organisms: Quantifying sensitivities and interaction with warming, Glob Chang Biol, 19, 1884–1896, https://doi.org/10.1111/gcb.12179, 2013.
- Legge, O., Johnson, M., Hicks, N., Jickells, T., Diesing, M., Aldridge, J., Andrews, J., Artioli, Y., Bakker, D. C. E., Burrows, M. T., Carr, N., Cripps, G., Felgate, S. L., Fernand, L., Greenwood, N., Hartman, S., Kröger, S., Lessin, G., Mahaffey, C., Mayor, D. J., Parker, R., Queirós, A. M., Shutler, J. et. al D., Silva, T., Stahl, H., Tinker, J., Underwood, G. J. C., Van Der Molen, J., Wakelin, S., Weston, K., and Williamson, P.: Carbon on the Northwest European Shelf: Contemporary Budget and Future Influences, Front Mar Sci, 7, https://doi.org/10.3389/fmars.2020.00143, 2020.
- Lehmann, N., Stacke, T., Lehmann, S., Lantuit, H., Gosse, J., Mears, C., Hartmann, J., and Thomas, H.: Alkalinity responses to climate warming destabilise the Earth's thermostat, Nat Commun, 14, https://doi.org/10.1038/s41467-023-37165-w, 2023.
 - Lewis, E., Wallace, D., and Allison, L. J.: Program developed for CO₂ system calculations, Oak Ridge National Laboratory (ORNL), https://doi.org/10.2172/639712, 1998.

- Li, X., Wu, Z., Ouyang, Z., and Cai, W.-J.: The source and accumulation of anthropogenic carbon in the U.S. East Coast, Sci Adv, 10, 3169, https://doi.org/10.1126/sciadv.adl3169, 2024.
 - Liu, Q., Dai, M., Chen, W., Huh, C. A., Wang, G., Li, Q., and Charette, M. A.: How significant is submarine groundwater discharge and its associated dissolved inorganic carbon in a river-dominated shelf system?, Biogeosciences, 9, 1777–1795, https://doi.org/10.5194/bg 9-1777-2012, 2012.
 - Lucker, T.Liang, H., Lunstrum, A. M., Dong, S., Berelson, W. M., and John, S. G.: Constraining CaCO₃ Export and Dissolution With an Ocean Alkalinity Inverse Model, Global Biogeochem Cycles, 37, https://doi.org/10.1029/2022GB007535, 2023.

 Lorkowski, I., Pätsch, J., DicksonMoll, A.-G., and Keeling, C. D.: Ocean pCO₂-calculatedKühn, W.: Interannual variability of carbon fluxes in the North Sea from dissolved inorganic carbon, alkalinity,1970 to 2006 Competing effects of abiotic and equations for K¹- and K²: validation basedbiotic drivers on laboratory measurements the gas-exchange of CO₂-in gas and seawater at equilibrium, Mar Chem, 70, 105–119, Estuar Coast Shelf Sci, 100, 38–57, https://doi.org/10.1016/S0304-4203(00)00022-0, 2000.

120

- Lüger, H., Wallace, D. W. j.ecss.2011.11.037, 2012 R., Körtzinger, A., and Nojiri, Y.: The *p*CO₂ variability in the midlatitude North Atlantic Ocean during a full annual cycle, Global Biogeochem Cycles, 18, https://doi.org/10.1029/2003GB002200, 2004.
- Luitjens, L.: Analytische Messung auserwählter Nährstoffkonzentrationen im ökologischen System Wattenmeer und Ems, sowie deren Entwicklung, Einflüsse und Auswirkungen, Unpublished master's thesis, 2019.
 - Macovei, V. A., Petersen, W., Brix, H., and Voynova, Y. G.: Reduced Ocean Carbon Sink in the South and Central North Sea (2014–2018) Revealed From FerryBox Observations, Geophys Res Lett, 48, 1–11, https://doi.org/10.1029/2021GL092645, 2021.
- Norbisrath, M., Van Beusekom, J. E. E., and Thomas, H.: Distribution and source attribution of alkalinity Alkalinity sources in the Dutch Wadden Sea, Biogeosciences Ocean Science, 20, 1423–1440, https://doi.org/10.5194/egusphere 2023-2595, 2023 os-20-1423-2024, 2024.
 - Onken, R. and Riethmüller, R.: Determination of the freshwater budget of tidal flats from measurements near a tidal inlet, Cont Shelf Res, 30, 924–933, https://doi.org/10.1016/j.csr.2010.02.004, 2010.
 - Orr, J. C., Fabry, V. J., Aumont, O., Bopp, L., Doney, S. C., Feely, R. A., <u>Gnanadesikan, A., Gruber, N., Ishida, A., Joos, F., Key, R. M., Lindsay, K., Maier-Reimer, E., Matear, R., Monfray, P., Mouchet, A., Najjar, R. G., Plattner, G. K., Rodgers, K. B., et. alSabine, C. L., Sarmiento, J. L., Schlitzer, R., Slater, R. D., Totterdell, I. J., Weirig, M. F., Yamanaka, Y., and <u>Yool, A.</u>: Anthropogenic ocean acidification over the twenty-first century and its impact on calcifying organisms, Nature, 437, 681–686, https://doi.org/10.1038/nature04095, 2005.</u>
- Pätsch, J. and Lenhart, H.: Daily Loads of Nutrients, Total Alkalinity, Dissolved Inorganic Carbon and Dissolved Organic Carbon of the European Continental Rivers for the Years 1977-2002, 48–159 pp., Berichte Aus Demaus dem Zentrum Fürfür Meeres- Undund Klimaforschung, Institut Für MeereskundeReihe B, Ozeanographie, 2004.

- Postma, H.: Exchange of materials between the North Sea and the Wadden Sea, Mar Geol, 40, 199–213, https://doi.org/10.1016/0025-3227(81)90050-5, 1981.
- Prowe, A. E. F., Thomas, H., Pätsch, J., Kühn, W., Bozec, Y., Schiettecatte, L. S., Borges, A. V., and de Baar, H. J. W.:

 Mechanisms controlling the air-sea CO₂ flux in the North Sea, Cont Shelf Res, 29, 1801–1808, https://doi.org/10.1016/j.csr.2009.06.003, 2009.
 - Redfield, A. C., Ketchum, B. H., and Richards, F. A.: The influence of organisms on the composition of seawater, The sea, 2, 26–77, 1963.
 - Ricour, F., Guidi, L., Gehlen, M., DeVries, T., and Legendre, L.: Century-scale carbon sequestration flux throughout the ocean by the biological pump, Nat Geosci, 16, 1105–1113, https://doi.org/10.1038/s41561-023-01318-9, 2023.

160

- Sabine, C. L., Feely, R. A., Gruber, N., Key, R. M., Lee, K., Bullister, J. L., Wanninkhof, R., Wong, C. S., Wallace, D. W. R., Tilbrook, B., Millero, F. J., Peng, T.-H., Kozyr, A., Ono, T., and Rios, A. F.: The Oceanic Sink for Anthropogenic CO₂, Science, (1979), 305, 367–371, https://doi.org/10.1126/science.1097403, 2004.
- Santos, I. R., Beck, M., Brumsack, H. J., Maher, D. T., Dittmar, T., Waska, H., and Schnetger, B.: Porewater exchange as a driver of carbon dynamics across a terrestrial-marine transect: Insights from coupled ²²²Rn and pCO₂ observations in the German Wadden Sea, Mar Chem, 171, 10–20, https://doi.org/10.1016/j.marchem.2015.02.005, 2015.
 - Schneider, A., Wallace, D. W. R., and Körtzinger, A.: Alkalinity of the Mediterranean Sea, Geophys Res Lett 34, https://doi.org/10.1029/2006GL028842, 2007.
 - Schulz, G., Sanders, T., Van Beusekom, J. E. E., Voynova, Y. G., Schöl, A., and Dähnke, K.: Suspended particulate matter drives the spatial segregation of nitrogen turnover along the hyper turbid Ems estuary, Biogeosciences, 19, 2007–2024, https://doi.org/10.5194/bg-19-2007-2022, 2022.
 - Schwichtenberg, F.: Drivers of the Carbonate System Variability carbonate system variability in the Southern North Sea: River Input, Anaerobic Alkalinity Generation input, anaerobic alkalinity generation in the Wadden Sea and Internal Processes internal processes, 2013.
 - Schwichtenberg, F., Pätsch, J., <u>Ernst Böttcher</u>, M.-E., Thomas, H., <u>and Winde</u>, V., <u>and Emeis, K. C.</u>: The impact of intertidal areas on the carbonate system of the southern North Sea, Biogeosciences, 17, 4223–4245, https://doi.org/10.5194/bg-17-4223-2020, 2020.
 - Staneva, J., Stanev, E. V., Wolff, J. O., Badewien, T. H., Reuter, R., Flemming, B., Bartholomä, A., and Bolding, K.: Hydroynamics and sediment dynamics in the German Bight. A focus on observations and numerical modelling in the East Frisian Wadden Sea, Cont Shelf Res, 29, 302–319, https://doi.org/10.1016/j.csr.2008.01.006, 2009.
 - Takahashi, T., Olafsson, J., Goddard, J. G., Chipman, D. W., and Sutherland, S. C.: Seasonal variation of CO₂ and nutrients in the high latitude surface oceans: A comparative study, Global Biogeochem Cycles, 7, 843–878, https://doi.org/10.1029/93GB02263, 1993.

- Takahashi, T., Sutherland, S. C., Sweeney, C., Poisson, A., Metzl, N., Tilbrook, B., et. al.: Global sea air CO₂ flux based on climatological surface ocean pCO₂, and seasonal biological and temperature effects, Deep Sea Research Part II: Topical Studies in Oceanography, 49, 1601–1622, https://doi.org/10.1016/S0967-0645(02)00003-6, 2002.
 - Talke, S. A. and De Swart, H. E.: Hydrodynamics and Morphology in the Ems/Dollard Estuary: Review of Models, Measurements, Scientific Literature, and the Effects of Changing Conditions, Institute for Marine and Atmospheric Research Utrecht, https://doi.org/http://archives.pdx.edu/ds/psu/11193, 2006.
- Thomas, H., Bozec, Y., Elkalay, K., <u>Dede</u> Baar, H. J. W., Borges, A. V_{7.4} and Schiettecatte, L.-S.: Controls of the surface water partial pressure of CO₂ in the North Sea, Biogeosciences, 2, 323–334, https://doi.org/10.5194/bg-2-323-2005, <u>2005a2005</u>.
 - Thomas, H., Prowe, A. E. F., van Heuven, S., Bozec, Y., Dede Baar, H. J. W., Elkalay, K., Frankignoulle, M., Schiettecatte, L. S., Kattner, G., and Suykens, K., Koné, M., Borges, A. V., Lima, I. D., :: The carbon budget and Doney, S. C.: Rapid decline of the CO₂ buffering capacity in the North Sea, Biogeosciences, 2, 87–96 and implications for the North Atlantic Ocean, Global Biogeochem Cycles, 21, https://doi.org/10.5194/bg 2 87 2005, 2005b1029/2006GB002825, 2007.

190

1195

- Thomas, H., Schiettecatte, L.-S., Suykens, K., Koné, Y. J. M., Shadwick, E. H., Prowe, A. E. F., Bozec, Y., <u>Dede</u> Baar, H. J. W., and Borges, A. V.: Enhanced ocean carbon storage from anaerobic alkalinity generation in coastal sediments, Biogeosciences, 6, 267–274, https://doi.org/10.5194/bg-6-267-2009, 2009.
- Tozawa, M., Nomura, UNESCO World Heritage Centre: https://whc.unesco.org/en/list/1314/, last access: 23 March 2025, n.d. D., Nakaoka, S. ichiro, Kiuchi, M., Yamazaki, K., Hirano, D., Aoki, S., Sasaki, H., and Murase, H.: Seasonal Variations and Drivers of Surface Ocean pCO₂ in the Seasonal Ice Zone of the Eastern Indian Sector, Southern Ocean, J Geophys Res Oceans, 127, https://doi.org/10.1029/2021JC017953, 2022.
 - Voynova, Y. G., Petersen, W., Gehrung, M., Aßmann, S., and King, A. L.: Intertidal regions changing coastal alkalinity: The Wadden Sea-North Sea tidally coupled bioreactor, Limnol Oceanogr, 64, 1135–1149, https://doi.org/10.1002/lno.11103, 2019.
- Weiss, R. F.: Carbon dioxide in water and seawater: the solubility of a non-ideal gas, Mar Chem, 2, 203-215, https://doi.org/10.1016/0304-4203(74)90015-2, 1974.
- Wolf-Gladrow, D. A., Zeebe, R. E., Klaas, C., Körtzinger, A., and Dickson, A. G.: Total alkalinity: The explicit conservative expression and its application to biogeochemical processes, Mar Chem, 106, 287–300, https://doi.org/10.1016/j.marchem.2007.01.006, 2007.
- Wolfstein, K., Colijn, FWu, C. S., Røy, H., and Doerffer, R.: Seasonal Dynamicsde Beer, D.: Methanogenesis in sediments of Microphytobenthos Biomass and Photosynthetic Characteristics an intertidal sand flat in the Northern German-Wadden Sea, Obtained by the Photosynthetic Light Dispensation System, Estuar Coast Shelf Sci, 51, 651 662164, 39–45, https://doi.org/10.1006/1016/j.ecss.2000.0702, 20002015.06.031, 2015.
- 1205 Xue, L. and Cai, W. J.: Total alkalinity minus dissolved inorganic carbon as a proxy for deciphering ocean acidification mechanisms, Mar Chem, 222, https://doi.org/10.1016/j.marchem.2020.103791, 2020.

Xue, L., Cai, W. J., Sutton, A. J., and Sabine, C.: Sea surface aragonite saturation state variations and control mechanisms at the Gray's Reef time-series site off Georgia, USA (2006–2007), Mar Chem, 195, 27–40, https://doi.org/10.1016/j.marchem.2017.05.009, 2017.